9-1-2020

Late-Holocene Shoreline Responses to Competing Shelf, Bay, and Beach Accommodation Spaces Under Conditions of Relative Sea Level Change, and the Potential for Future Catastrophic Beach Retreat in the Columbia River Littoral Cell, Washington and Oregon, USA

Curt D. Peterson
Portland State University, curt.d.peterson@gmail.com

Tamara C. Linde
Cascade Radon, Inc.

Sandy Vanderburgh
Kwantlen Polytechnic University

Citation Details

Peterson, C. D., Linde, T. C., & Vanderburgh, S. (2020). Late-Holocene shoreline responses to competing shelf, bay, and beach accommodation spaces under conditions of relative sea level change, and the potential for future catastrophic beach retreat in the Columbia River Littoral Cell, Washington and Oregon, USA. Marine Geology, 106272.

Marine Geology 427 (2020) 106272

Contents lists available at ScienceDirect

Marine Geology

journal homepage: www.elsevier.com/locate/margo

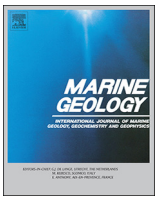

Late-Holocene shoreline responses to competing shelf, bay, and beach accommodation spaces under conditions of relative sea level change, and the potential for future catastrophic beach retreat in the Columbia River Littoral Cell, Washington and Oregon, USA

Curt D. Peterson[a,*], Tamara C. Linde[b], Sandy Vanderburgh[c]

[a] Geology Department, Portland State University, Portland, OR 97207, USA
[b] Cascade Radon, Inc, Portland, OR 97230, USA
[c] Kwantlen Polytechnic University, Surrey, British Columbia V3W2M8, Canada

A B S T R A C T

The Columbia River Littoral Cell (CRLC) (160 km in length) provides opportunities to compare competing accommodation space relations under different conditions of relative sea level change. The CRLC system includes abundant littoral sand supply from the large Columbia River, late-Holocene prograded beach plains and barrier spits (0.5–5 km in width), two large marine-dominated estuaries (Willapa Bay and Grays Harbor), and a high-wave-energy inner-shelf. Littoral sand accumulation rates in prograded beach plains and barrier deposits are based on paleo-shoreline positions that are dated by great-earthquake catastrophic beach retreat scarps (n = 10) from 0.3 to 5.0 ka. The retreat scarp timelines are mapped in across-shore GPR transects (n = 79), yielding timeline-bounded polygons (n = 247). The polygons are evaluated for littoral sand volume and bounding ages, yielding volume accretion rates ($m^3\ ka^{-1}$), which are summed for the four CRLC subcells; Clatsop Plains ($27.4 \times 10^6\ m^3\ ka^{-1}$), Long Beach ($19.8 \times 10^6\ m^3\ ka^{-1}$), Grayland Plains ($15.9 \times 10^6\ m^3\ ka^{-1}$), North Beaches ($11.7 \times 10^6\ m^3\ ka^{-1}$). Major submarine sinks of littoral sand, including the inner-shelf and large marine-dominated estuaries, are evaluated for increased littoral sand accommodation space that could result from potential future sea level rise of 1, 2 and 3 m during the next century or two. The estimated beach and nearshore sand erosion needed to fill the increased submarine accommodation space from a 2.0 m rise in relative sea level would result in averaged beach retreat values of ~0.7 km (Clatsop Plains), ~1.2 km (Long Beach), and ~ 1.3 km (Grayland Plains), about 30–50% larger than previous estimates based on the Brunn method. These catastrophic shoreline retreat distances (0.7–1.3 km) represent 25–50% of the present widths of prograded barrier spits and beach plains. They serve as warnings about future catastrophic beach erosion resulting from potential future SLR in other similar barrier spit and beach plain shorelines worldwide.

1. Introduction

The Columbia River Littoral Cell (CRLC) (Fig. 1) includes the extraordinary coincidences of high wave-energies, abundant littoral sand supply, and reversing relative sea level changes from subduction zone neotectonics, as superimposed on longer-term eustatic sea level rise. These conditions have previously been used to constrain accommodation space controls on littoral sand accumulation rates in 1) the upper-shoreface under the prograded barrier spits and beach plains (Herb, 2000; Vanderburgh et al., 2010; Peterson et al., 2010a), 2) the inner-shelf (Twichell and Cross, 2001; Twichell et al., 2010; Peterson et al., 2016), and 3) the large mesotidal estuaries (Peterson et al., 2013; Peterson and Phipps, 2016; Peterson and Vanderburgh, 2018a, 2018b). In this article, the littoral sand volumes that were partitioned in the CRLC barrier spits and beach plains (0.5–5 km in width) are used to demonstrate the complex interplays between the shelf, bays, and beaches in competition for available littoral sand supplies, during latest-Holocene time (3–0 ka). These relationships are used in this study to predict responses of high-wave-energy sandy-shorelines to potential future conditions of sea level rise (SLR) from ongoing global warming (Kopp et al., 2014; Bamber et al., 2019; Kopp et al., 2019).

Partitioned littoral sand volumes in the four subcells of the CRLC system (Fig. 1) are based on coseismic beach retreat scarps that provide timelines (200–800 yr recurrence intervals) throughout the length of the littoral system (Meyers et al., 1996; Woxell, 1998; Peterson et al., 2010b). Littoral sand accumulation rates for specific time intervals and associated relative sea level changes during late-Holocene time (5–0 ka) range widely between the four different subcells (Linde, 2014). Sand volumes that were partitioned into each of the four subcells during corresponding time intervals are compared in this article for 1) across inner-shelf gradients (slopes), 2) shoreline orientations relative to dominant wave forcing, and 3) intervening estuary sand sinks. The prograded shoreline accretion rates are compared to corresponding fill rates in the inner-shelf and in the large marine-dominated estuaries

* Corresponding author.
E-mail addresses: curt.d.peterson@gmail.com (C.D. Peterson), sandy.vanderburgh@kpu.ca (S. Vanderburgh).

https://doi.org/10.1016/j.margeo.2020.106272
Received 17 September 2019; Received in revised form 11 May 2020; Accepted 9 June 2020
Available online 11 June 2020

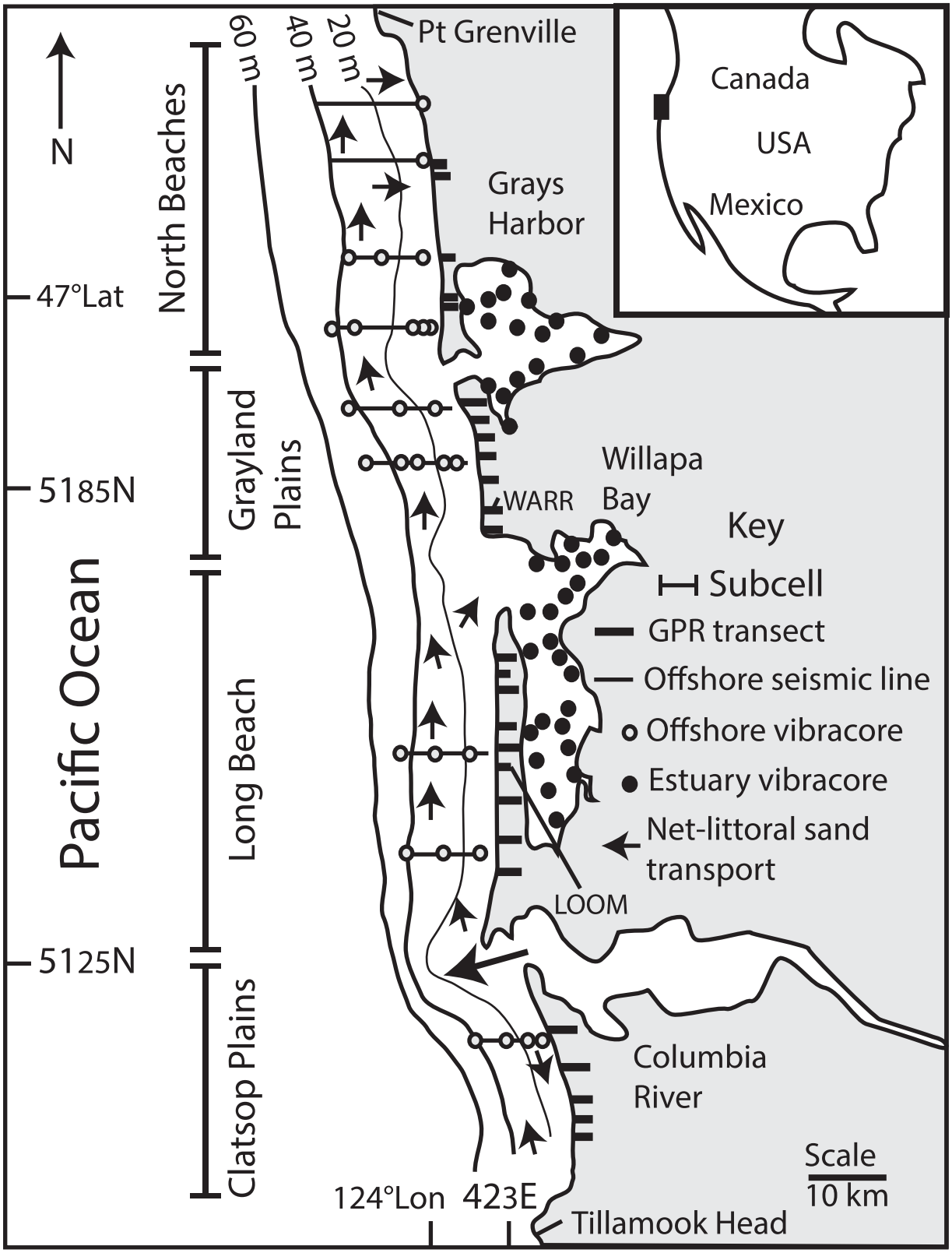

Fig. 1. Location of the Columbia River Littoral Cell (CRLC) including 1) bounding headlands (Point Grenville, Tillamook Head), 2) subcell beach segments (Clatsop Plains, Long Beach, Grayland Plains, North Beaches), 3) inner-shelf bathymetric contours (20 m, 40 m, 60 m water depth), 4) onshore ground penetrating radar (GPR) transects, 5) offshore seismic lines, 6) selected inner-shelf vibracores, 7) estuary vibracores, and 8) interpreted net-littoral sand transport directions (arrows). The Columbia River mouth supplied the Holocene littoral sand to the CRLC system. Littoral sand sinks include the inner-shelf, Willapa Bay, Grays Harbor, and the prograded subcell barriers and beach plains. GPR transects, including WARR and LOOM, are from Peterson et al. (2010b). Offshore seismic lines are from Twichell et al. (2010). Selected offshore vibracores are from Kaminsky (2006). Beach toe vibracore/drill sites are from Vanderburgh et al. (2010) and Peterson et al. (2016). Estuary vibracores in Willapa Bay and Grays Harbor, respectively, are from Peterson and Vanderburgh (2018a) and Peterson and Vanderburgh (2018b). Littoral sand transport directions are from Peterson et al. (2010a) and Peterson et al. (2016).

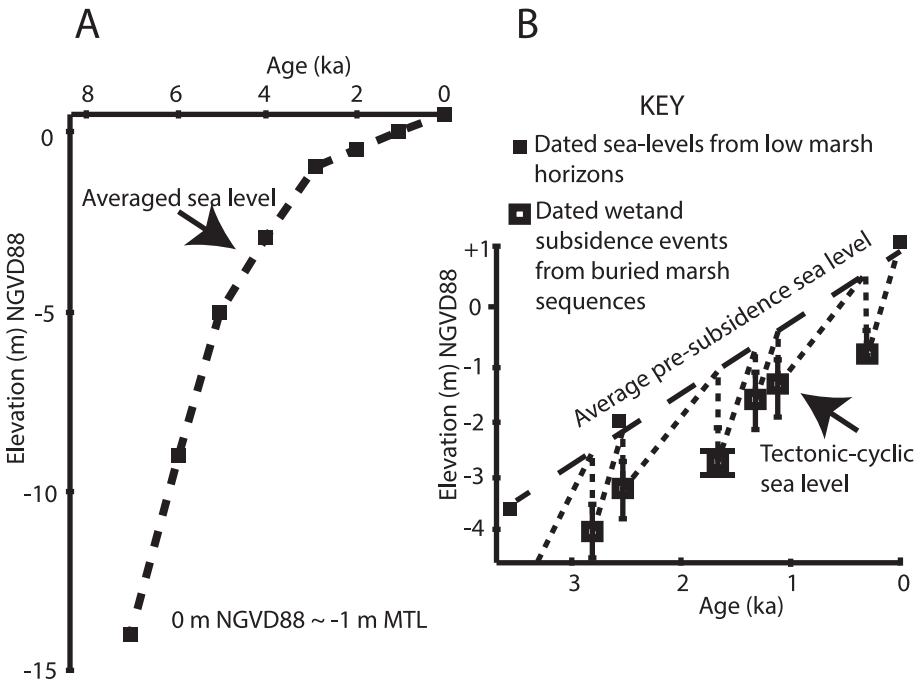

Fig. 2. Sea level curves from the CRLC system. Part A. Averaged sea level curve (dashed line) in middle- to late-Holocene time (8–0 ka). The regional NAVD88 elevation datum (0 m) is equivalent to about −1.0 m mean tidal level (MTL). Figure is redrafted from Peterson et al. (2010a). Part B. High-resolution sea level curve for latest-Holocene time (3–0 ka) including average sea level (dashed line) and neotectonic 'cyclic' sea levels (dotted line) from coseismic subsidence and interseismic uplift. Subsidence events from youngest to oldest correspond to retreat scarp timelines (Table 2) as follows A (0.3 ka), B (1.1 ka), C (1.3 ka), D (1.7 ka), E (2.5 ka), and F (2.8 ka). Figure is redrafted from Peterson and Vanderburgh (2018a).

(Willapa Bay and Grays Harbor), under longer-term time scales (millennial) of net SLR. Reversals of relative sea level occur over shorter time scales (decades to centuries) and resulted in widespread reversals of catastrophic beach retreat and then recovery. Such short time scales are based on previously reported ages of beach erosion and accretion associated with the last subduction zone neotectonic cycle (1700 CE to the present) (Woxel, 1998; Phipps et al., 2001; Peterson et al., 2000). The relative sea level changes (0.5–2.0 m) forced by the neotectonic cycles in the study area also resulted in episodic accretion of littoral sand in shallow tidal flats of the large marine-dominated estuaries, Willapa Bay and Grays Harbor (Peterson and Vanderburgh, 2018a, 2018b). Because the potential shoreline retreat rates for the larger SLR scenarios (2 and 3 m) are so large in the CRLC system we use the known past beach accretion to apportion the estimated beach erosion and associated shoreline retreat distances following predicted future SLR.

The sequences of littoral sand accumulation that are documented in this study are used 'in reverse' to yield beach erosion sequences under conditions of future SLR (1–3 m), as predicted to potentially occur during the next century or two (Jevrejeva et al., 2012; DeConto and Pollard, 2016; Mengel et al., 2016; Kopp et al., 2019). Predicted sequences and volumes of beach erosion in the CRLC are based on established littoral sand transfers to more competitive sand sinks or increasing marine accommodation spaces in the inner-shelf and the large marine-dominated estuaries, under conditions of net SLR. Accommodation spaces for littoral sand in those competing sand sinks will increase with future SLR at the same time that decreasing accommodation spaces in the onshore (beach) settings will cause shoreline destabilization and retreat. As shown for the high-energy CRLC system, such sand transfers to the inner-shelf and marine-dominated estuaries did occur at the one or two century time scales or at about the durations of possible near-future SLR scenarios as proposed here. The relations reported here, for the sand-rich CRLC system, serve as warnings for high-wave-energy shorelines world-wide that could experience catastrophic erosion of barrier spits and broad beach plains under potential future conditions of sustained global SLR.

2. Background

2.1. Littoral sand sources and dispersal in the CRLC system

The Columbia River littoral cell system (160 km in length) contains four subcells including the Clatsop Plains, Long Beach Spit, Grayland Plains and North Beaches (Fig. 1). The subcells are separated by large tidal inlets of the intervening estuaries; Columbia River, Willapa Bay, and Grays Harbor. The larger CRLC system is bounded by the small headlands, Tillamook Head (south), and Point Grenville (north). Through-put of hypersthene-rich Columbia River sand to the littoral zone (Baker et al., 2010; Peterson et al., 2013) filled the submerged inner-shelf and marine-dominated estuaries in mid-Holocene time (Vanderburgh et al., 2010; Twichell et al., 2010; Peterson and Phipps, 2016; Peterson et al., 2016). The initial filling of those accommodation spaces then led to progradation of the barrier spits and beach plains in late-Holocene time (Woxell, 1998; Vanderburgh et al., 2010; Peterson et al., 2010a, 2010b). The Holocene Columbia River sand was transported north and south of the Columbia River mouth by nearshore and inner-shelf longshore transport within, and between, the adjoining subcells (Fig. 1). There is no evidence of late-Pleistocene shelf sand (augite-rich) being delivered to the late-Holocene prograded barriers and beach plains or to the large marine-dominated estuaries by the Holocene marine transgression. Pre-transgressive shelf sand deposits were swept north of the CRLC system by strong northward littoral transport along the shelf during late-Pleistocene and early-Holocene marine low-stands. A northward shift of storm tracks during Holocene time (Alder and Hostetler, 2015; Peterson et al., 2016) diminished the strong net-northward littoral transport, yielding only slightly net-northward sand transport from the Columbia River mouth in late-Holocene time (5–0 ka).

2.2. Sea level curves for the CRLC system

Reported sea level curves for the CRLC system are shown in Fig. 2. Long-term net SLR slows from ~7 m ka^{-1} in middle-Holocene time to ~1.0 m ka^{-1} in latest-Holocene time. The onset of barrier and beach plain net-progradation in the CRLC system, at 5–4 ka (Rankin, 1983; Woxell, 1998; Peterson et al., 2010a, 2010b), corresponds to the

substantial decrease in the rate of SLR, at 5–4 ka (Fig. 2 Part A). Due to the neotectonic forcing of relative SLR in the study area (Atwater et al., 2004), the relative sea level changes follow step-like patterns of cyclic coseismic subsidence and interseismic uplift (~1.0 ± 0.5 m vertical). These shorter-term neotectonic cycles are supper-imposed on the longer-term conditions of eustatic net SLR (Fig. 2 Part B). The short-term cyclic patterns of relative sea level change are established from buried tidal marsh or supratidal forest sequences, as regionally correlated by near-field paleo-tsunami inundation and ^{14}C dating in Grays Harbor, Willapa Bay, and the Columbia River estuary (Darienzo et al., 1994; Jurney, 2001; Atwater et al., 2004). The interseismic intervals of sea level change are likely more complicated than those shown in Fig. 2 Part B, including the early-and late-stages of little to no uplift and the intervening middle-stages of sustained tectonic uplift (Cruikshank and Peterson, 2017).

2.3. Beach and estuary response to cyclic coseismic subsidence and interseismic uplift

Catastrophic beach-retreat scarps are mapped throughout the CRLC from ground penetrating radar (GPR) profiles and ground-truthing with auger borehole and/or vibracore sampling (Fig. 1) (Meyers et al., 1996; Woxell, 1998). The retreat scarps resulted from regional coseismic subsidence events (0.5–2.0 m) (Fig. 2 Part B), which are correlated to ^{14}C-dated tidal marsh burial sequences in adjacent estuaries (Atwater and Hemphill-Haley, 1997; Peterson et al., 2010b). Retreat scarps cross-cut or truncate seaward-dipping beach face layers that formed during preceding interseismic intervals (200–800 yr durations) of beach face progradation (Jol et al., 1999). Retreat scarp depths (generally 3–10 m below prograded beach plain surfaces) are imaged by ground penetrating radar (GPR) and ground-truthed by heavy-mineral lag deposits, as recovered in auger and/or vibracore boreholes (Fig. 3).

The landward distances of the catastrophic beach retreats are not directly measured, due to erosional losses of the pre-subsidence shoreline positions. However, beach retreat from the last coseismic subsidence event at 1700 has been estimated using Bruun's relations (Bruun, 1962; Doyle, 1996; Peterson et al., 2000). Assuming a 1.5 m rise in relative sea level and 17.5 m interannual depth of closure, the measured across-shore profiles yield calculated retreat values of ~300 m in distance. Doyle (1996) also considered greater values of coseismic subsidence (2.0 m) and interannual depth of closure (20 m), as discussed later, in Section 5.6. Most of the beach retreat, following coseismic subsidence, is assumed to have taken place during the early-stage, or first several decades, of the interseismic cycle, as interpreted below. Where sufficient interseismic progradation occurred between the coseismic retreat events, the preserved sequence of ^{14}C dated retreat scarps provide timelines of net upper-shoreface progradation (Fig. 4 Part A).

The duration of catastrophic beach retreat, following the last coseismic subsidence event in the Cascadia subduction zone at 1700 CE (Satake et al., 1996), is constrained by the earliest ages of foredune reactivation in prograded barriers and beach plains of the CRLC system. The foredune reactivation and abrupt abandonment by beach progradation, respectively, reflect the onset and then acceleration of beach recovery during the tectonic uplift portion or the middle stage of the interseismic interval (Cruikshank and Peterson, 2017). Such records of post-1700 dune reactivation have been reported for 14 sites in the CRLC subcells (Woxell, 1998). Particularly well-developed dune reactivation records occur in the WARR and WASH profiles, and the adjacent Washaway Beach cut-bank section, located along the north side of the Willapa Bay tidal inlet (Fig. 1 and Fig. 4 Part A**).** Thick sand layers (1–3 m in thickness) above a weak paleosol (soil A-horizon) in the WARR and WASH profiles greatly exceed thin sand layers (1–5 cm thick) produced by paleotsunami sand transport in the adjacent inter-dune valley bogs (Schlichting and Peterson, 2006). Such thick dune sand layers rule-out foredune dune reactivation by paleotsunami inundation, as initially proposed by Phipps et al. (2001). Numerous trees/stumps were rooted in the pre-1700 paleosol and/or overlying dune deposits, as represented by sample sites BD, WASH8 and WASH5 (Fig. 4 Part B). Radiocarbon dating of the dune-buried trees/stumps yield approximate kill dates, calibrated (1σ) median ages (Calib7.10, 2019), of 181 cal BP (site BD) (Phipps et al., 2001), and 184 cal BP (site WASH8)

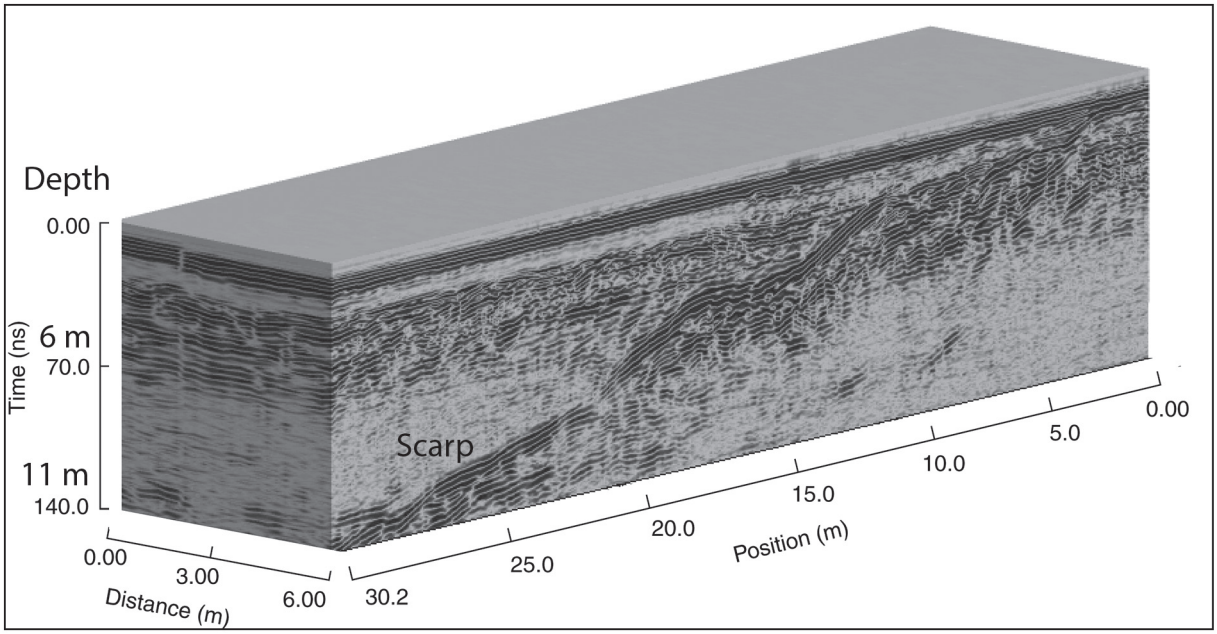

Fig. 3. Ground penetrating radar 3D image of a very-large beach retreat scarp (high-amplitude reflections) resulting from a coseismic subsidence event (~2.0 m subsidence), dated to ~1.7 ka in the LOOM transect in the Long Beach subcell (Fig. 1) (Meyers et al., 1996; Jol et al., 2003; Peterson et al., 2010b). The erosional scarp (dipping seaward to image left) is enhanced by iron-rich heavy mineral lag deposits, which were ground-truthed for depth and extent by auger drilling and/or vibracoring. A calibrated two-way signal velocity (0.08 m ns^{-1}) yields a scarp scour depth of 11 m below surface and subsequent prograded beach facies to 6 m depth below surface, in this image. The site surface elevation (road) is ~7 m above the 0 m NAVD88 vertical datum. The 0 m NAVD88 datum is about 1.0 m below present mean sea level (MSL) in the study area. The imaged retreat scarp cut about 4 m below the post-subsidence paleo-sea level during the period of abrupt retreat.

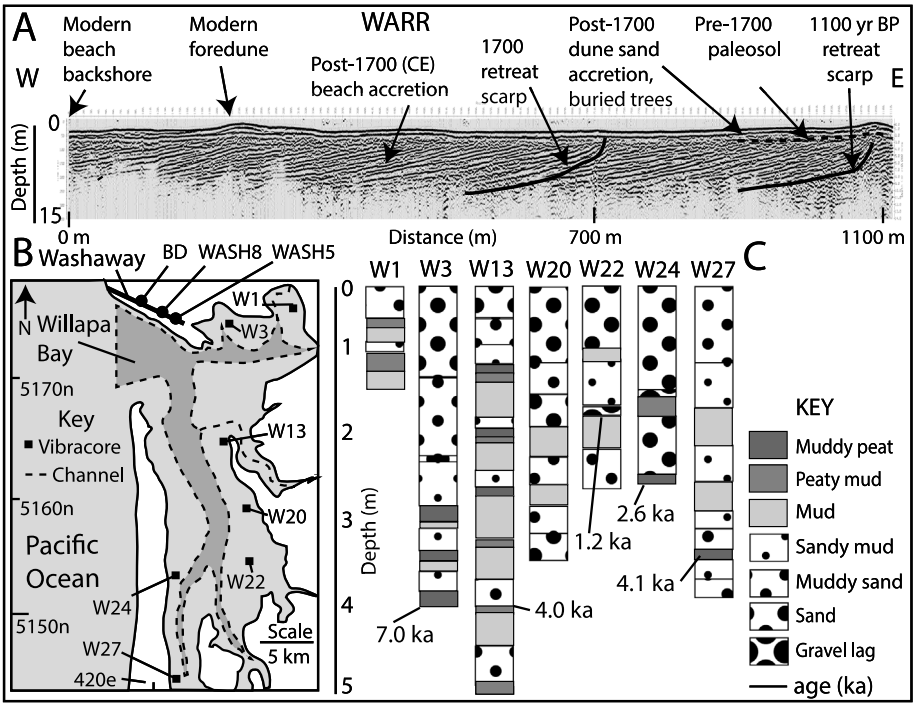

Fig. 4. Part A. GPR profile (WARR), located north of the Willapa Bay tidal-inlet cut-bank (Fig. 1) (Peterson et al., 2010b). The GPR profile includes the last two catastrophic retreat scarps (bold lines) at 1700 CE and 1100 yr BP. Boreholes define a dune-buried paleosol (dashed line) between the underlying pre-1700 foredune and the overlying post-1700 accreted dune sand deposits. Part B. Map of Willapa Bay showing the Washaway GPR profile and adjacent cut-bank exposure (solid line) with sand buried trees/stumps (sold circles) at sites BD (Phipps et al., 2001) and WASH8 and WASH5 (Woxell, 1998). Selected vibracore sites (solid squares) are plotted in the shallow tidal flats of Willapa Bay. Part C. Representative vibracore logs from Willapa Bay show basin-wide littoral sand accumulation (stippled patterns) above episodically-subsided wetlands (shaded patterns). Net SLR (Fig. 2 Part B) preserves only some subsidence/uplift cycles under conditions of longer-term tidal flat transgression in Willapa Bay (Peterson and Vanderburgh, 2018a).

and 184 cal BP (site WASH5) (Woxell, 1998). Adjusting for 0 yr ^{14}C age at 1950, the average calendar age (CE) for the three prehistoric tree stumps is 1767, or ~ 70 years after the 1700 subsidence event. Catastrophic beach retreat and associated offshore sand transport likely occurred within several decades of the 1700 subsidence event in the high-wave-energy CRLC system. The onset of beach recovery and dune reactivation, prior to 1770, probably coincided with the beginning of the middle stage (~1750) of the interseismic interval (Cruikshank and Peterson, 2017).

Following the initial post-1700 foredune reactivation, wide-spread beach progradation ensued in the CRLC barriers sand beach plains (Fig. 4 Part A). The progradation abandoned the reactivated foredunes, developing the backshore flats between the prehistoric foredune and modern foredunes. The relatively rapid beach progradation, between ~1750–1885, was likely forced by 1) regional onshore sand transport, following tectonic uplift and 2) localized gradients in along-shore sand transport, following river sand throughput to the littoral zone from the Columbia River mouth. However, the rates of beach accretion greatly accelerated after 1885 throughout nearly all of the CRLC system (Woxell, 1998). The natural conditions of beach sand supply in the CRLC system were greatly altered in the early 1900s due to anthropogenic impacts from 1) grazing, logging, and agriculture in the Columbia River tributary drainage basins and 2) jetty construction and offshore dredge spoil disposal at the Columbia River and Grays Harbor estuary mouths (Sherwood et al., 1990; Kaminsky et al., 2010). Sediment retention rates from numerous impoundments of the Columbia River tributaries (1950s to present) are not established. Although these anthropogenic impacts are important to regional sediment management practices, they do not clarify the relations of shoreline responses to changing marine accommodation spaces resulting from relative SLR, so they are not further addressed in this article.

Littoral sand supplies to the large marine-dominated estuaries, Willapa Bay and Grays Harbor, responded to the neotectonic cycles of coseismic subsidence and interseismic uplift. For example, post-subsidence accumulations of littoral sand layers at 13 tidal flat sites in Willapa Bay (Fig. 4 Parts B and C) averaged 0.5 m thickness for 30 post-subsidence sequences (Peterson and Vanderburgh, 2018a). It is assumed that most of the littoral sand that was transported into the shallow tidal flats of Willapa Bay and Grays Harbor occurred during the relatively brief periods (< 100 years) of substantial submergence (≥1.0 m), following the coseismic subsidence events (Peterson and Vanderburgh, 2018a, 2018b). However, the long-term net SLR (1.0 m ka^{-1}) during latest-Holocene time (3–0 ka) permitted the influx and net deposition of littoral sand in the marine dominated estuaries, Willapa Bay and Grays Harbor (Table 1). Late-Holocene accumulation rates of littoral sand are estimated to be 110 × 10^6 m^3 ka^{-1} in the Willapa Bay tidal flats and 117 × 10^6 m^3 ka^{-1} in the Grays Harbor tidal flats and tidal channels. Littoral sand sinks in the subtidal channels

Table 1
Late-Holocene rates of littoral sand supply and accumulation (sinks) in the CRLC system.

Settings	Surface area (km^2)	Littoral sand supply (×10^6 m^3 ka^{-1})	Littoral sand sink (×10^6 m^3 ka^{-1})
Columbia River throughput	–	5000 *3200	–
Prograded shoreface	300	–	860
Willapa Bay	347	–	110
Grays Harbor	236	–	650
Inner-shelf	1600	–	2100
Total	–	–	3720

Notes: The estimated rate of Columbia River sand throughput to the littoral zone (5000 × 10^6 m^3 ka^{-1}) is based on decreasing sedimentation rates in the Lower Columbia River Valley between middle and late Holocene time (Peterson et al., 2013). A second method (*) of estimating Columbia River sand throughput to the marine side in Holocene time is based on the total net accumulation rate, as summed from all of the measured CRLC sand sinks (total is 3720 × 10^6 m^3 ka^{-1}). Littoral sand sinks or net accumulation rates in the prograded barriers, beach plains, and the underlying upper-shoreface deposits (7–0 ka) are from Herb (2001) and Peterson et al. (2010a). Littoral sand sinks or accumulation rates, in Grays Harbor averaged about 650x10^{6}m^3 ka^{-1} during Holocene time (Peterson and Phipps, 2016). Littoral sand accumulation rates in Willapa Bay are only known for latest-Holocene time (110 × 10^6 m^3 ka^{-1}) (Peterson and Vanderburgh, 2018a). Littoral sand accumulation rates in the inner-shelf (0–50 m water depth or ~ 10 km inner-shelf width) are based on Holocene (12–0 ka) fill rates above the marine transgressive ravinement surface (Peterson et al., 2016).

of Willapa Bay have not been established, but they could be substantial as they represent about 45% of the surface area in Willapa Bay. The neotectonic cycles of coseismic subsidence and interseismic uplift are also recorded in buried wetland sequences around the margin of the Columbia River estuary (Peterson and Cruikshank, 2014). Such buried wetland sequences were not preserved in the interior areas of the Columbia River estuary due to frequent channel lateral migrations and deposit reworking (Peterson et al., 2014). The roles of short-term episodic submergence and emergence in controlling river sand accumulation or bypassing in the Columbia River estuary are not known. However, increased accommodation space for river sand in the estuary, following episodic subsidence (Fig. 2 Part B), could have temporarily reduced river sand throughput to the littoral zone (see further discussion in Section 5.5).

Frequent storm-wave reworking of offshore deposits in the inner-shelf by large storm surf (peak wave height 10–12 m) (Ruggiero et al., 1997) apparently precluded any stratigraphic evidence of neotectonic forcing of littoral sand accumulation in the inner-shelf (Kaminsky, 2006). Nevertheless, the inner-shelf served as 1) a short-term reservoir of the littoral sand that was removed from the beaches following coseismic subsidence events and 2) the major long-term sink of littoral sand (2100×10^6 m^3 ka^{-1}) in the CRLC system during Holocene time (Table 1) (Twichell et al., 2010; Peterson et al., 2016). Although some littoral sand was lost from the inner-shelf to the middle-shelf (> 50 m water depth) and from the southern Washington shelf to the northern Washington shelf (Fig. 1), during early- and middle-Holocene time (Peterson et al., 2010a) the inner-shelf was likely a more effective trap of Columbia River sand delivered to the CRLC system during late-Holocene time (Peterson et al., 2016).

3. Methods

Previously reported beach-retreat scarps (160 in number) (Peterson et al., 2010b) in shore-normal GPR profiles (Fig. 1) were connected by straight or simple curved lines to form shore-parallel timelines in the CRLC prograded barriers and beach plains (Linde, 2014). Including the modern shoreline (0 m NAVD88 elevation contour), a total of 11 timelines, ranging from 0 to 5.0 ka, were constructed in the CRCL subcells (Table 2). The 0 m NAVD88 datum (time 0 ka) is approximately 1.0 m below modern mean sea level (MSL) in the study area. The orientation and continuity of the proposed timelines were verified by semi-continuous shore-parallel foredune segments, as shown in Lidar digital elevation models (Lidar DEM), where the foredune segments did not locally bifurcate, converge, or offset (Linde, 2014). The mostly-orthogonal intersections of the across-shore GPR profiles with shore-parallel timelines generally formed rectangular polygon cells (Fig. 5 Part A). However, more complex cell boundaries occur at tidal inlets. The intersecting GPR profiles, shore-parallel timelines, and tidal inlet shorelines were used to map 247 polygon cells in the prograded barriers and beach plains of the CRLC system (Linde, 2014).

Table 2
Retreat scarp time lines in the CRLC system.

Retreat scarp timeline	Estimated age (ka)	Estimated subsidence (m)	Retreat scarp size (m)
Modern	0	–	–
A	0.3	1.5	5–10
B	1.1	1.0	3–7
C	1.3	0.5	~3
D	1.7	2.0	8–12
E	2.5	0.5	~3
F	2.8	1.0	5–10
G	3.2	1	5–10
H	4.0	–	3–7
I	4.7	–	5–10
J*	5.0	–	3–7

Notes: Along-shore timelines are constructed between corresponding catastrophic beach retreat scarps (letters), which have been previously assigned to approximate age (ka) and estimated coseismic subsidence (m) (Peterson et al., 2010b). Retreat scarp size (m) is taken (vertically) from the most landward (shallowest) truncated beach strata elevation to the most seaward (deepest) truncated beach strata or heavy-mineral (placer lag) deposit. Retreat scarp vertical extents (minimums based on GPR reflections) are interpreted from 79 GPR lines comprising 35 across-barrier/beach plain profiles in the CRLC system (Peterson et al., 2010b). The J timeline (*) is arbitrarily mapped along the back-edges of the prograded barrier-spits and beach plains, thereby possibly over-representing volume accretion during the 'assumed' 4.7–5.0 ka time interval.

Though retreat scarps are locally inclined or seaward dipping (Fig. 3), the polygon cell timeline-boundaries are extended vertically downward (Fig. 5 Part B). The vertically projected timelines form straight sided polygon cells that simplify cell volume calculations. Average polygon cell heights (top surface elevations), including abandoned foredunes and interdune valleys, were established by ArcGIS averaging of bare-ground Lidar digital elevation models (Lidar DEM). The bare-ground Lidar datasets, including thirty-two 1/9 arc sec NED files (Gesch et al., 2002) as surveyed from 2001 to 2005, were stitched together in ArcGIS to form one seamless base file (Linde, 2014). The top surface averaging accounts for all irregularities associated with locally developed foredune ridge and intervening valley topographies. The polygon cell bottoms (basal elevations) are based on projected paleo-beach toe elevations, starting with the modern beach toe (0 ka) at 0 m NAVD88. The prehistoric beach toe elevations were estimated for corresponding timelines, based on the latest-Holocene rate of sea level change (1.0 m ka^{-1}) (Fig. 2). The polygon cell bottom elevation is taken as an average of the two paleo-beach toe elevations that correspond to the two bounding retreat scarp timelines (Table 3). For purposes of bounding the onset location and age of the most-landward polygon cells, the timeline preceding the first recorded retreat scarp is mapped at 1) the barrier spit bay shoreline or 2) the beach plains back-edge or base of hill slope (Linde, 2014). The most-seaward extents of the historic polygon cells (1700 to modern) are mapped at the 0 m NAVD88 elevation datum (Lidar DEM) or the modern beach toe (Ruggiero et al., 2005). Where sequential retreat scarps or timelines are missing in a GPR transect, possibly due to subsequent subsidence event erosion, the two closest preserved retreat scarps are used as bounding timelines, as shown in Table 3. Polygon cell thicknesses (average top -to- average bottom elevations) were multiplied by polygon cell surface areas to yield accreted sand volumes in the polygon cells. Sand grain-size data from numerous borehole samples in the CRLC barrier and beach plains are provided in Woxell (1998), Herb (2000), and Peterson et al. (2010a, 2010b).

Each of the 247 mapped polygon cells (Fig. 6) was assigned a centroid (ArcGIS calculated center point) with position coordinates (NAD83 UTM sector 10 N) in a MSAccess™ relational database. Additional polygon attributes were linked to the centroids in the database tables (Linde, 2014). The centroid attributes include UTM east and UTM north (m), mean elevation (m), minimum age (yr BP), maximum age (yr BP), mean centroid age (yr BP), surface area (m^2), average thickness (m), and volume (m^3). The attributes for all 247 centroids in the four subcells (North Beaches, Grayland Plains, Long Beach, and Clatsop Plains) are summarized in four spreadsheet files (CentroidData.xls), as presented in Supplementary Data. Error estimates are as follows: retreat scarp position, as projected vertically (± 25 m in UTM NAD83), retreat scarp (timeline) age (± 75 yr), polygon cell centroid position (± 10 m), polygon cell elevations (± 1 m), as reported by Linde (2014).

In re-analysis of shoreline retreat estimates resulting from past episodes of SLR in the CRLC beaches (Doyle, 1996) it became apparent that a means was needed by which to apportion future sand volume loss from the modern shorelines following large (2–3 m) values of SLR. Such associated retreat distances could exceed several hundred meters in the existing barrier and beach plain widths. A guide is needed to predict what sequences of barrier and beach plain sand losses would occur in

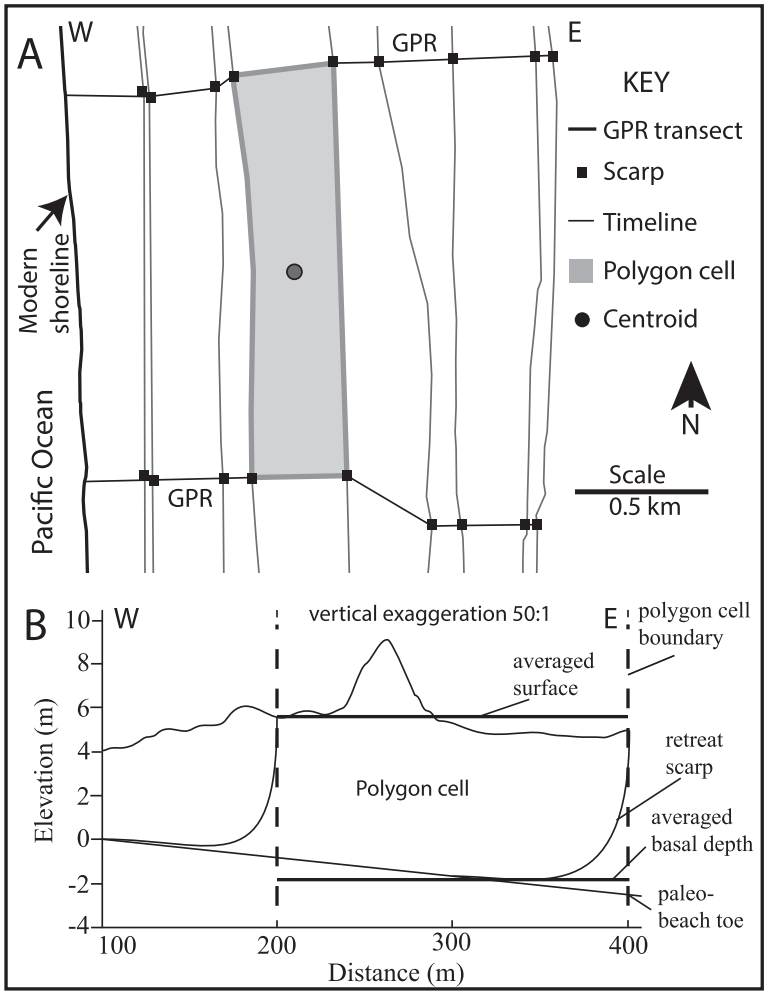

Fig. 5. Part A. Map view of polygon cell (shaded) defined by retreat scarps (solid squares) in GPR transects (bold line) and digitized timelines between corresponding retreat scarps. The timelines are guided by, or digitized parallel to, continuous abandoned foredune ridges, which are assumed to represent shoreline orientations prior to foredune abandonment. The center of the mapped polygon cell is assigned a unique centroid (solid circle), with defined position coordinates, and corresponding polygon cell attributes imported into a relational database (Microsoft Access™). Part B. Cross-section of a polygon cell (boxed) defined by vertically-extended retreat scarp timelines (dashed lines), an averaged surface elevation (bold line) from ArcGIS analysis of Lidar digital elevation models (LDEM), and an averaged basal depth (bold line) from the average of timeline intersections with a paleo-sea level curve. The sea level curve (gradient 1.0 m ka^{-1}) is normalized to the modern beach toe at 0 m NAVD88 (Linde, 2014), so it represents paleo-beach toe elevations at dated retreat scarps or timelines. Vertical exaggeration is 50:1.

Table 3
Mean ages and projected basal depths of polygon cell centroids.

Timeline interval	Polygon cell age (years)	Calculated basal depth (m NAVD88)
Modern/A	150	−0.15
A/B	700	−0.70
A/C*	800	−0.80
B/C	1200	−1.20
B/D*	1400	−1.40
C/D	1500	−1.50
D/E	2100	−2.10
E/F	2650	−2.65
E/G*	2850	−2.85
F/G	3000	−3.00
G/H	3600	−3.60
F/I*	3750	−3.75
H/I	4350	−4.35
I/J	4850	−4.85

Notes: In rare cases a retreat scarp was missing within a mapped polygon cell (*), so mean centroid age was determined by the closest existing retreat scarp ages. The mean age of the polygon cell was used to calculate the basal depth (m NAVD88) of the polygon cell, based on paleo-beach toe projections from the late-Holocene sea level change rate (1.0 m ka^{-1}) as shown in Fig. 2 Part B.

the CRLC system. To that end, recent past sequences of dated beach accretion in the CRLC subcells (Linde, 2014) are used 'in reverse' to evaluate most likely sequences of future sand losses and associated shoreline retreats in the CRLC shorelines, following future SLR. The dated sequences of late-Holocene barrier and beach plain accretion are presented below in the Results Sections (4.1–4.5). These results are then used in combinations with estimated sand sinks in the inner-shelf and large marine-dominated estuaries to predict shoreline erosion sequences, as presented below in the Discussion sections (5.1–5.6).

4. Results

In this section, the CRLC prograded barrier spits and beach plains are divided into 247 polygon cells, as based on across-shore GPR transects and age-correlative catastrophic beach retreat scarps. The polygon cells are analyzed for measured attributes including center (centroid) position coordinates, mean ages, and accreted sand volumes.

4.1. Mapped timelines in the CRLC barrier spits and beach plains

Modern foredunes that front the CRLC barrier spits and beach plains develop at the furthest landward distance of winter (storm) wave runup at the back-edge of the beach backshores. The modern foredune ridge crests are uniformly shore-parallel, both in straight beach segments (Fig. 7) and in the more complex or curved shorelines, such as those that occur at the ends of recurved spits. The modern foredunes developed over multiple years to decades so they represent time- and distance-averaged shoreline orientations, rather than seasonally ephemeral shoreline morphologies associated with beach cusps, rip heads, and/or attached swash bars. Although the modern and late-historic foredune ridges locally bifurcate, converge, and/or show small lateral offsets, their distance-averaged orientations are uniformly shore-parallel. Abandoned foredune ridges in the prograded CRLC barriers and

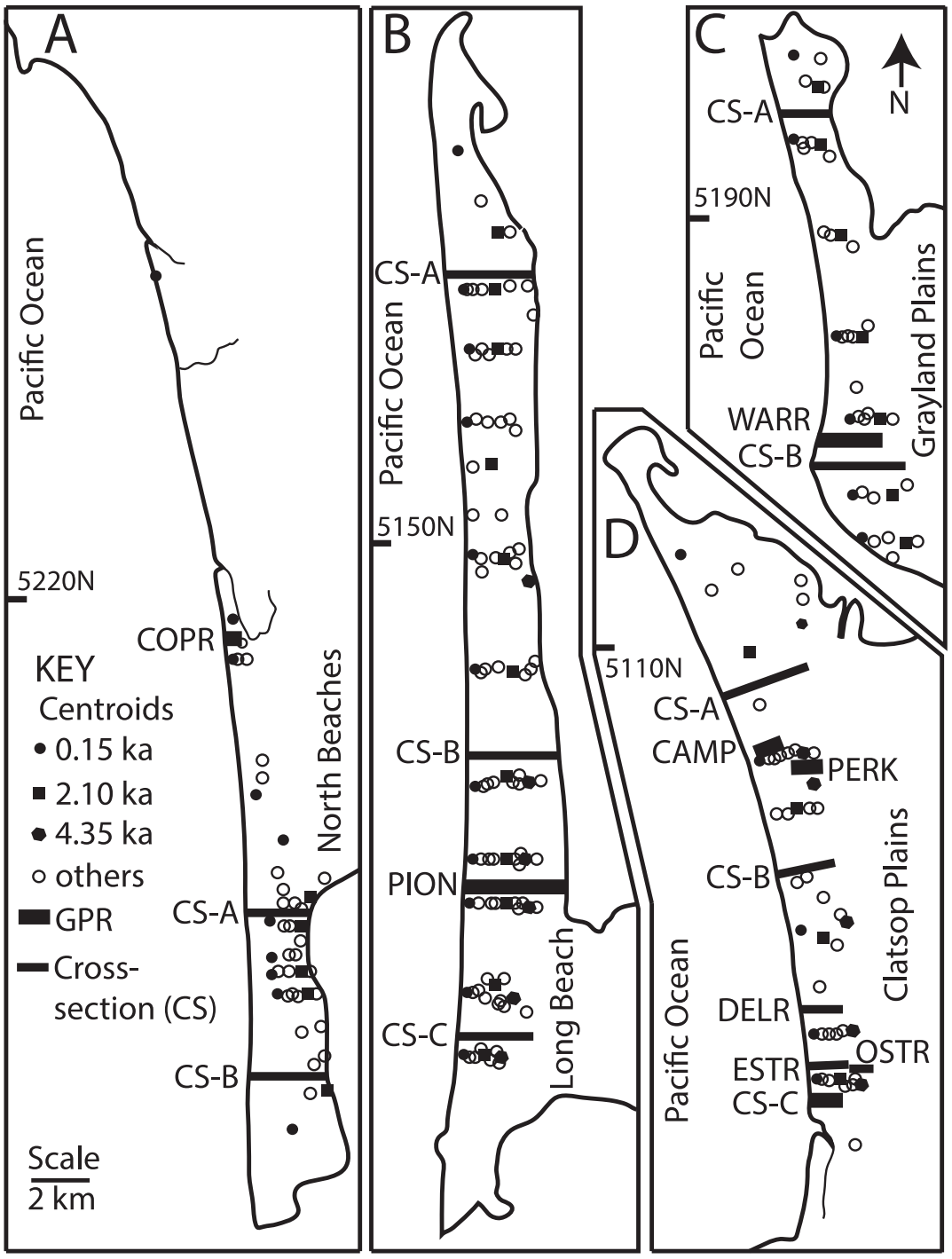

Fig. 6. Potted locations of 247 polygon cell centroids in prograded barrier spits and beach plains are shown for the North Beaches subcell (Part A), Long Beach subcell (Part B), Grayland Plains subcell (Part C) and Clatsop Plains subcell (Part D). Representative centroids are identified for timeline intervals and corresponding mid-point ages, including Mod/A at 0.15 ka or historic time (solid circles), D/E at 2.10 ka (solid squares), and H/I at 4.35 ka (solid hexagons). All other centroid intervals are identified by open circles. See Table 3 for polygon centroid ages. Centroid position coordinates, mid-point ages, and other attributes for the four CRLC subcells are presented in four summary databases (CentroidData.xls) in Supplementary Data. UTM northings are in kilometers. See Fig. 1 for the subcell locations in the study area.

beach plains are therefore assumed to represent paleo-shoreline orientations during corresponding periods of shoreline stability or modest accretion, as presented below.

The abandoned foredunes in the prograded CRLC barriers and beach plains were associated with episodic periods of shoreline stability between events of catastrophic retreat and rapid progradation (Fig. 4 Part A). However, due to the variations in progradation and retreat distances within different neotectonic cycles, the preserved foredune ridge sequences (Reckendorf et al., 2001) do not show a one-to-one correspondence with catastrophic retreat scarp sequences. Whereas the abandoned foredune ridges do not directly correlate by number to great earthquake cycles in the CRLC system, they do serve as guides to paleo-shoreline orientations during net accretionary phases of the barrier spits and beach plains. Continuous and distinct foredune ridges are used

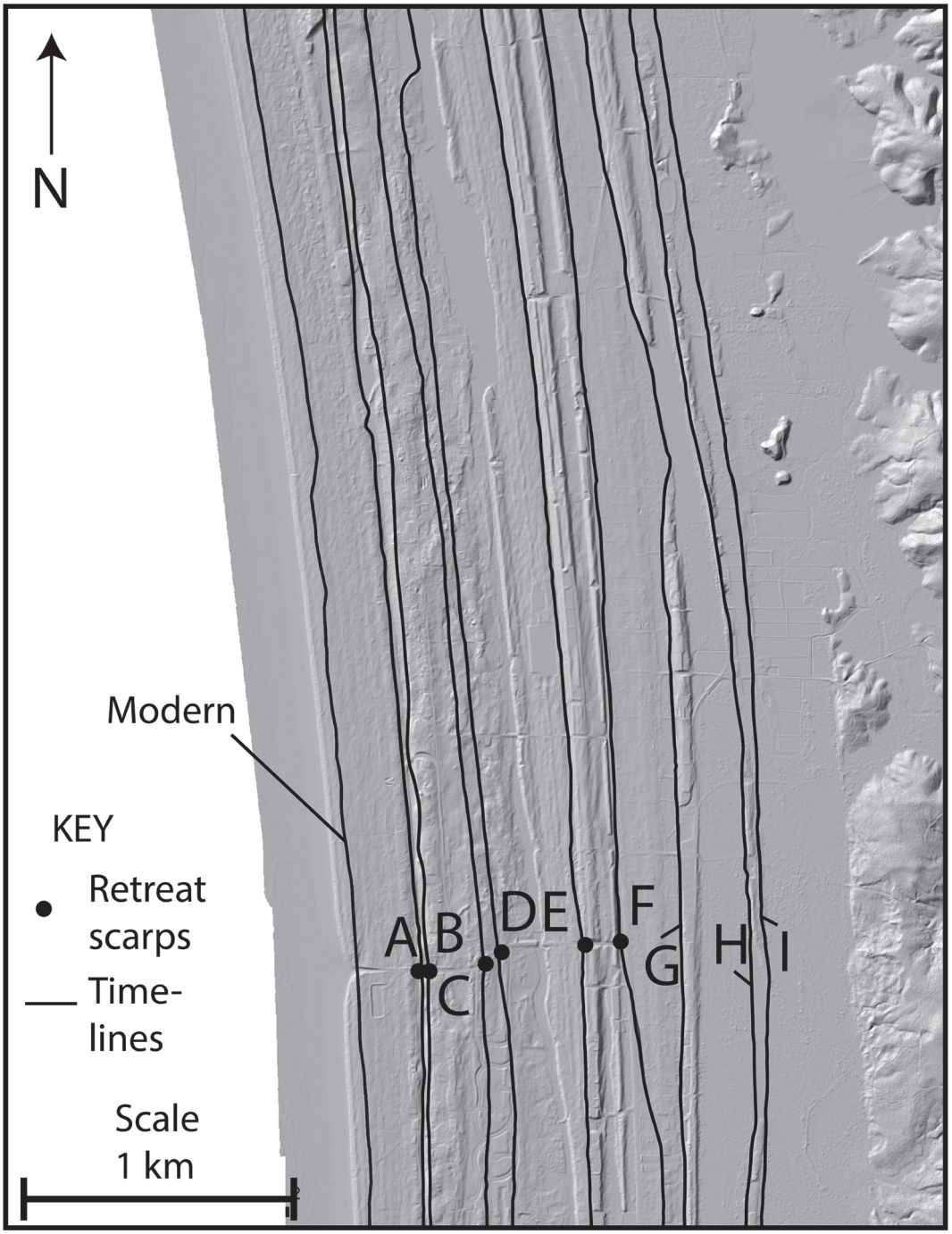

Fig. 7. Hill-shaded topographic relief map based on bare-ground Lidar DEM showing the modern or late-Historic foredune ridge (bold line at left side) and abandoned linear foredune ridges in the Clatsop Plains subcell (DELR transect in Fig. 6). Great earthquake retreat scarps (A-F) are plotted along the GPR transect DELR (Peterson et al., 2010b) that terminates to the east (landward) at submerged interdune valleys (bogs). Continuous distinct linear dune ridges were used to bridge timelines (G, H, I) to retreat scarps in longer GPR transect extensions (ESTR-OSTR) located to the south of the DELR transect. See Table 2 for ages of retreat scarps and corresponding timelines.

infrequently in this study to 1) bridge between longer GPR transects where shorter GPR transects were terminated in back barrier bogs (Fig. 7) and 2) to extend timelines beyond GPR transects where submerged bogs and/or tidal sloughs precluded GPR surveys (Fig. 8). Such extensions of timelines by abandoned dune ridges were only used in terminal spit areas, as located adjacent to the tidal inlets of the Columbia River, Willapa Bay, and Grays Harbor estuaries (Linde, 2014). The modern estuary shorelines (0 ka) are used to bound the polygon cell timelines that terminate at tidal inlets, as shown in Fig. 8.

4.2. Cross-sections in the CRLC barrier spits and beach plains

Selected across-shore profiles of the CRLC barrier spit and beach plain surfaces, as based on Lidar DEMs (Linde, 2014), are plotted together with corresponding paleo-beach toe basal elevations to construct representative cross-sections of the prograded beach and dune deposits (Figs. 9 and 10). The approximate positions of the last coseismic catastrophic retreat scarps, representing timeline 'A' at 1700 (Fig. 4 Part A), are shown, as projected to the high-resolution Lidar DEM profiles from

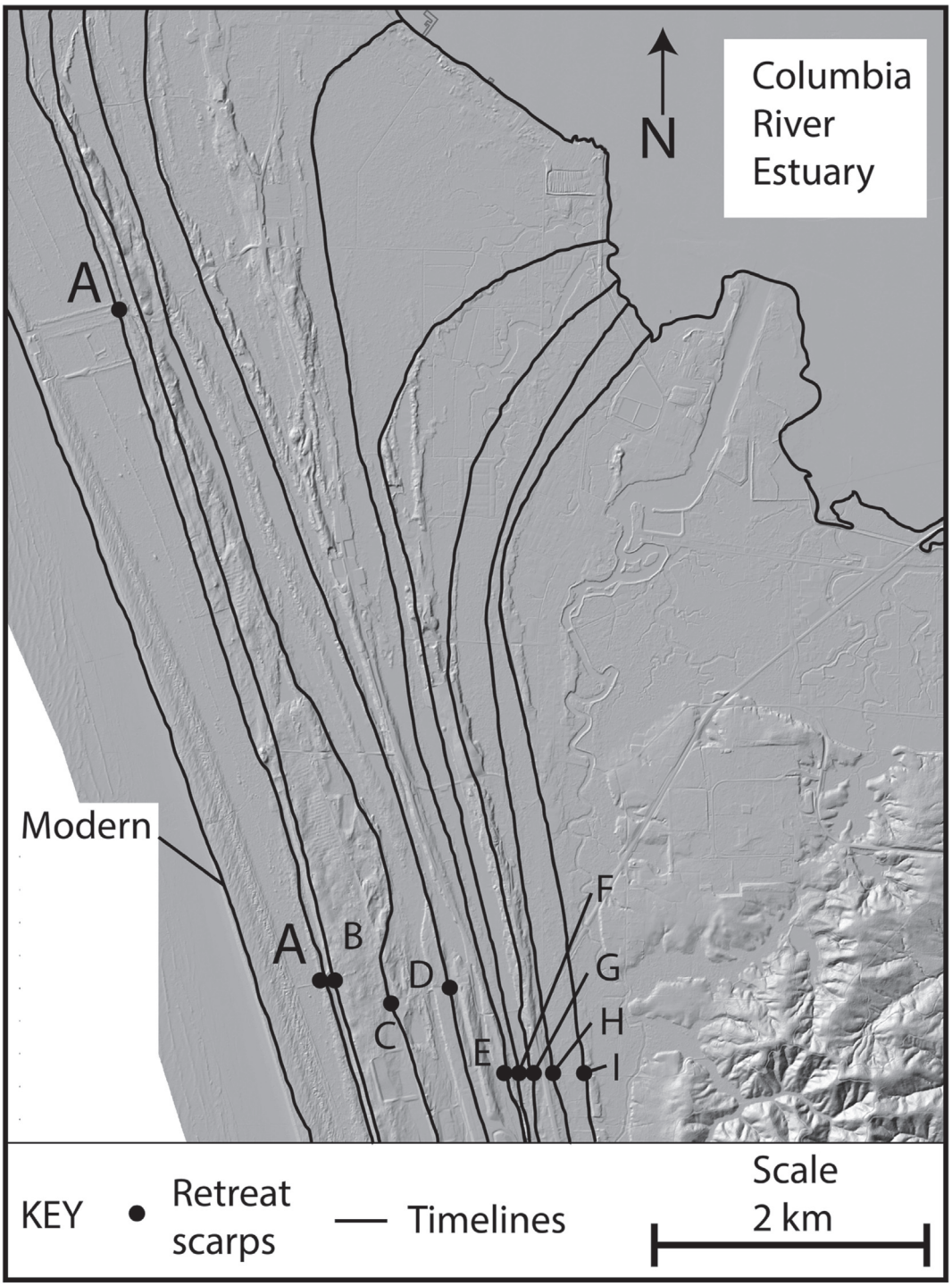

Fig. 8. Hill-shaded topographic relief map based on bare-ground Lidar DEM showing multiple late-Historic foredune ridges (located seaward of the 'A' timeline) and abandoned pre-historic foredune ridges (located landward of the 'A' timeline) in the northern part of the Clatsop Plains subcell (GPR transects CAMP and PERK in Fig. 6). The modern estuary shoreline (bold line) at the south side of the Columbia River mouth is used as an arbitrary boundary for the timeline terminations. Reported retreat scarps (A-I) are plotted along the two GPR transects (CAMP and PERK) that crossed the full width of the prograded beach plain (Peterson et al., 2010b). Submerged bogs and tidal sloughs precluded GPR surveying of the northernmost end of the Clatsop Plains. However, distinct semi-continuous foredune ridges were used to extend corresponding timelines to the Columbia River tidal inlet (Linde, 2014). See Table 2 for ages of retreat scarps and corresponding timelines.

the nearest GPR transects (Peterson et al., 2010b). In the North Beaches subcell, the only substantial shoreline progradation (> 500 m) occurred in the north spit of the Grays Harbor estuary (Fig. 6). Most of that progradation occurred during early historic time (early 1900s), following jetty construction and shoreline realignment (Kaminsky et al., 2010). The very-rapid historic progradation largely precluded foredune development in the two North Beach cross-sections (A and B). In contrast, most of progradation in the low-elevation Long Beach barrier spit (averaging ~6 m elevation) occurred during pre-historic time (pre-1700). The net progradation began at about 5 ka and 3 ka, respectively, at the south and north ends of the Long Beach barrier spit (Vanderburgh et al., 2010; Peterson and Vanderburgh, 2018a). The Grayland Plains

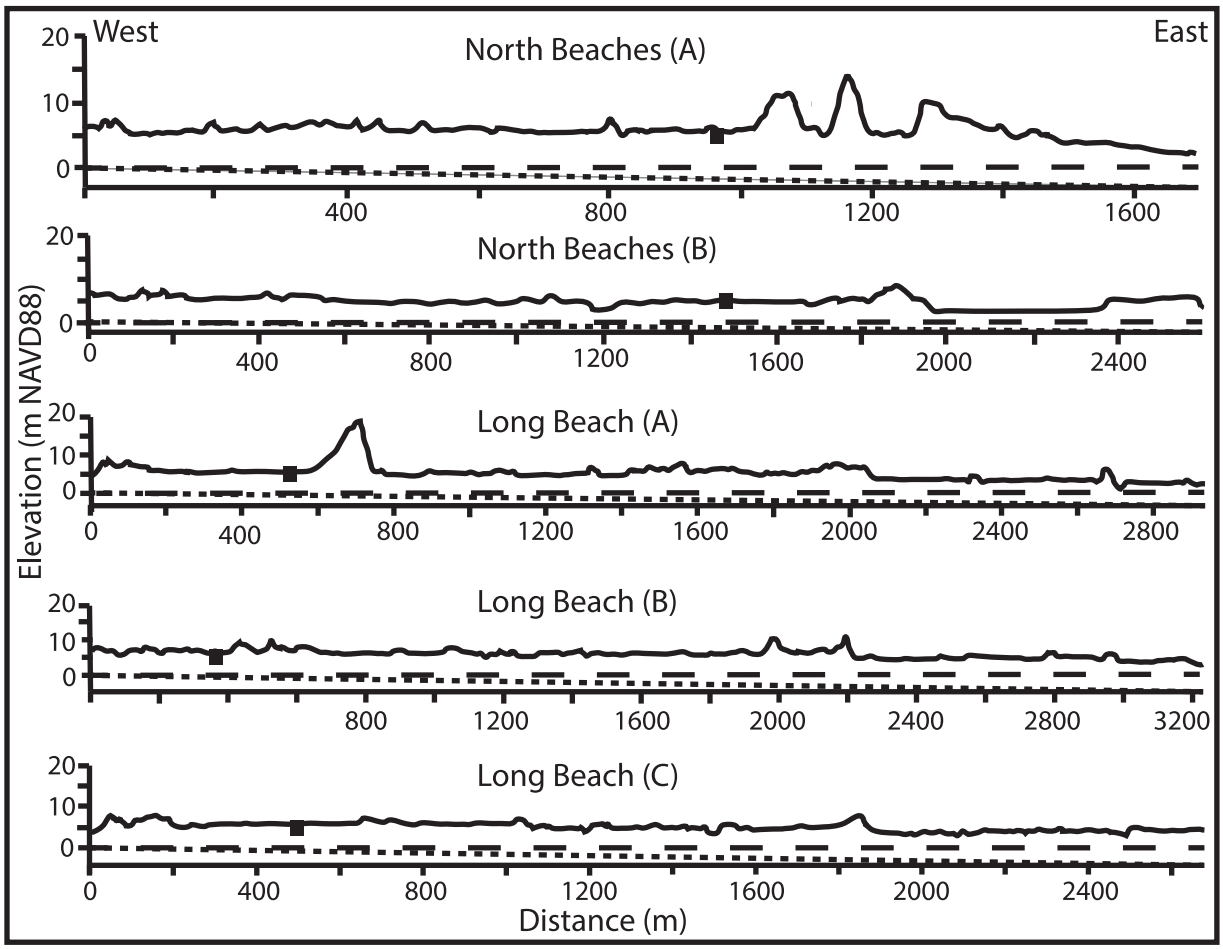

Fig. 9. Across-shore cross-sections of prograded barrier spits in the North Beaches and Long Beach subcells. Cross-sections include 1) top surface, 2) 0 m NAVD88 datum at the modern beach toe (dashed line), and the elevations of paleo-beach toes (dotted line) as projected landward from a sea level change of 1 m ka^{-1} in late-Holocene time (Fig. 2). The positions of 1700 retreat scarp or timeline A (solid square) are approximated from the nearest GPR transects (Peterson et al., 2010b). Vertical exaggeration for all cross-sections is 10:1. See Fig. 6 for the cross-section locations in the North Beaches and Long Beach subcells.

are also relatively low in surface elevation, though two large abandoned foredunes (10–15 m elevation) occur in the northern Grayland Plains cross-section (A). By comparison to the northern subcells in the CRLC system, the Clatsop Plains are characterized by abundant large foredunes, reaching 20–30 m in elevation. A combination of prolonged backshore sand supply and modest rates of net shoreline progradation permitted the development of large foredunes in the Clatsop Plains subcell, located south of the Columbia River mouth.

4.3. Polygon cell attributes in the CRLC barrier spits and beach plains

Centroid locations, bounding timeline ages, and volume accretion data, are established for 247 mapped polygon cells in the CRLC prograded barrier spits and beach plains (Fig. 6**)**. The number of digitized polygon cells in the four subcells range from 43 (Grayland Plains) to 97 (Long Beach) (Table 4). Average cell surface areas range from 707,833 m^2 (North Beaches) to 1,078,018 m^2 (Clatsop Plains). Average cell thickness ranges from 6.8 m (North Beaches and Grayland Plains) to 12.3 m (Clatsop Plains). The calculated averages of cell sand volumes are as follows; 11,270,668 m^3 (Clatsop Plains), 7,251,318 m^3 (Long Beach), 5,266,772 m^3 (Grayland Plains), and 3,894,488 m^3 (North Beaches).

4.4. Summed sand volumes within paired timelines for the four CRLC subcells

The summed volumes of sand accretion within bounding, or paired, timelines for each of the four CRLC subcells are presented in Table 5. The accreted sand volumes for the youngest prehistoric interval, bounded by the A/B timelines (0.3–1.1 ka), are 21.5 × 10^6 m^3 (Clatsop Plains), 22.1 × 10^6 m^3 (Long Beach), 18.8 × 10^6 m^3 (Grayland Plains), and 9.4 × 10^6 m^3 (North Beaches). These volumes are modest by comparison to the historic interval (Modern/A), which are greater than the A/B interval volumes by some 5–10 times (5–10×). The next older prehistoric interval, B/C at 1.1–1.3 ka, is represented by slightly larger volumes in the Clatsop Plains (> 31.1 × 10^6 m^3), Long Beach (760.0 × 10^6 m^3), and Grayland Plains (25.6 × 10^6 m^3), even though the B/C interval of 0.2 ka) is four times shorter than the A/B interval of 0.8 ka (Table 2). The A/B interval included two large coseismic events, and associated shoreline retreats, but the 'C' retreat scarps are amongst the smallest recorded in the CRLC (Table 2). These relations point to the importance of both the timing (duration) and scale (volume) of on-shore/offshore transport reversals, in controlling net beach accretion volumes over short time intervals. The variability in Columbia River sand throughput to the littoral zone over such short time scales (century) is not known, but it could also be influenced by the neotectonic cycles of coseismic subsidence and interseismic uplift. Averaging beach volume accretion data over multiple time intervals reduces the event-response resolution, but it clarifies the relative effectiveness of the four

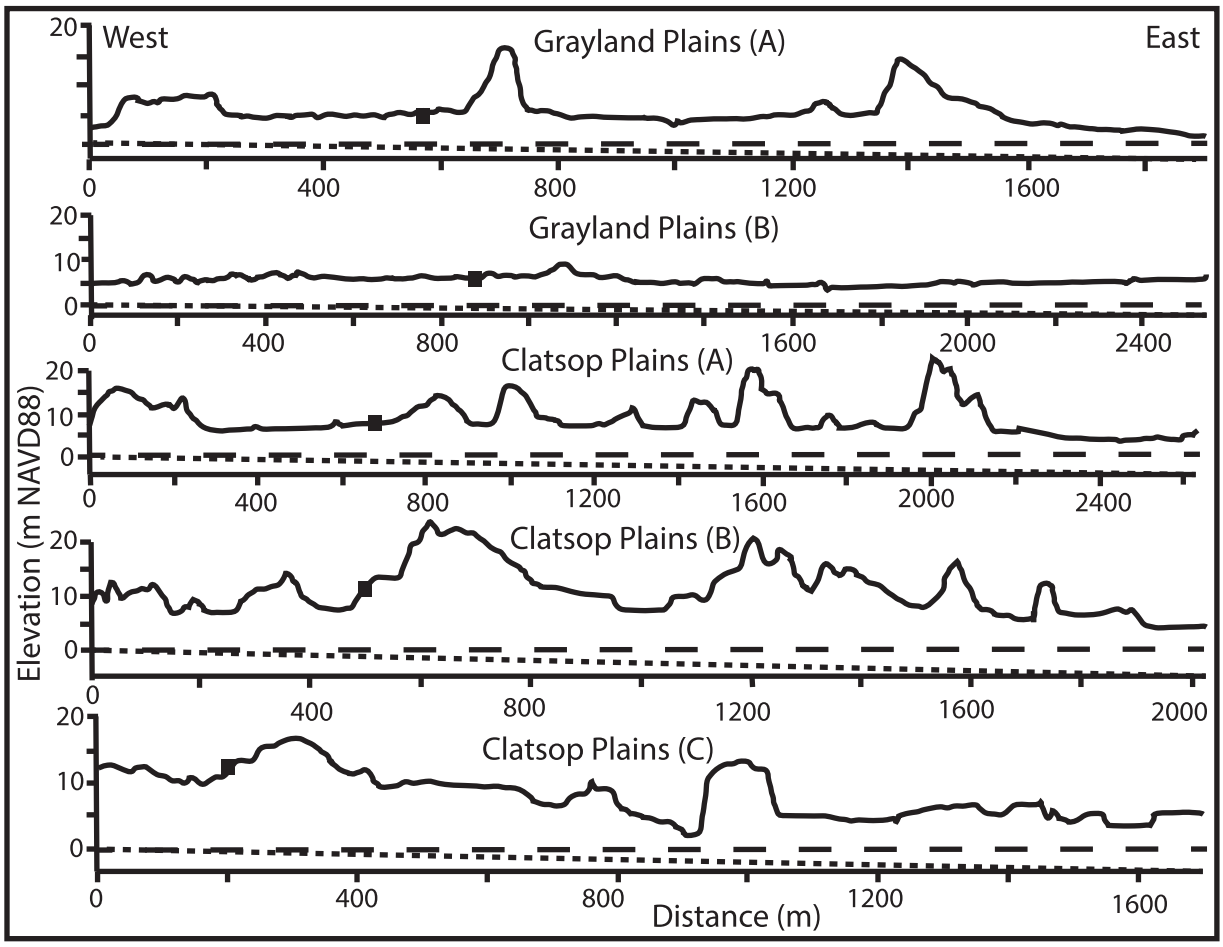

Fig. 10. Across-shore cross-sections of beach plains in the Grayland Plains and Clatsop Plains subcells. Cross-sections include 1) top surface, 2) 0 m NAVD88 datum at the modern beach toe (dashed line), and 3) the elevations of paleo-beach toes (dotted line) as projected landward from a sea level change of 1 m ka^{-1} in late-Holocene time (Fig. 2). The positions of 1700 retreat scarp or timeline A (solid square) are approximated from the nearest GPR transects (Peterson et al., 2010b). Vertical exaggeration for all cross-sections is 10:1. See Fig. 6 for the cross-section locations in the Grayland Plains and Clatsop Plains subcells.

subcells in competing for littoral sand supplies in the CRLC system. The longest time interval represented by net barrier and beach plain progradation in each subcell yields total beach-sand accretion volumes of 597.3 × 10^6 m^3 (Clatsop Plains), 703.4 × 10^6 m^3 (Long Beach), 231.7 × 10^6 m^3 (Grayland Plains) and 210.3 × 10^6 m^3 (North Beaches). The total beach/dune sand accretion volume for the summed subcells during late-Holocene time (5–0 ka) is 1742.8 × 10^6 m^3. See Tables 2 and 4 for subcell ages.

4.5. Average shoreline-normalized volume accretion rates in the four CRLC subcells

The relative effectiveness of littoral sand accumulation in the four CRLC subcells is addressed from normalizing 1) the timeline interval accreted sand volumes by subcell alongshore distance (m) and 2) the measured accumulation by interval duration (yr), to yield shoreline-normalized volume accretion rates (m^3 m^{-1} yr^{-1}) (Table 6, Fig. 11). The oldest timeline interval I/J is only represented in the Long Beach subcell, where the very-high rate there (23.5 m^3 m^{-1} yr^{-1}), might reflect some uncertainty about the back-edge age of the prograded barrier spit. A similar uncertainty exists for the timeline interval (E/F) in North Beaches subcell and in the rapidly-prograded Columbia River spit in the Clatsop subcell. With those exceptions, and the anomalously-narrow A/B intervals in all four subcells, the shoreline-normalized accretion rates generally increase through time in the CRLC prograded barriers and beach plains.

Some striking aspects of the dated shoreline progradations in the CRLC system are the late onset ages of accretion at timeline intervals F/G (3.2–2.8 ka) and E/F (2.8–2.5 ka), respectively, in the two northernmost subcells, North Beaches and Grayland Plains (Table 6, Fig. 11).

Table 4
Summary of polygon cell parameters for the four CRLC sub-cells.

Sub-cell Name	Retreat scarps (timelines) present	Number of polygon cells	Average cell surface area (m^2)	Average cell thickness (m)	Average cell volume (m^3)
Clatsop Plains	A-J	53	1,078,018	12.3	11,270,668
Long Beach Peninsula	A-J	97	907,870	8.4	7,251,318
Grayland Plains	A-F	43	805,486	6.8	5,266,772
North Beaches	A-G	54	707,833	6.8	3,894,488

Notes: Ages of coseismic catastrophic retreat scarps or time lines 'A–J' are presented in Table 2. Data are summarized from centroid database files for the Clatsop Plains, Long Beach, Grayland Plains, and North Beaches subcells (see CentroidData.pdf files in Supplementary Data).

Table 5
Volume totals (km^3) for each of the timeline intervals within the CRLC subcells.

Timeline interval	Clatsop Plains ($\times 10^6$ m^3)	Long Beach ($\times 10^6$ m^3)	Grayland Plains ($\times 10^6$ m^3)	North Beaches ($\times 10^6$ m^3)	Total volume ($\times 10^6$ m^3)
Modern/A	109.5	144.9	77.7	151.4	483.5
A/B	21.5	22.1	18.8	9.4	71.8
A/C	N.A.[a]	N.A.[a]	N.A.[a]	6.5	6.5
B/C	31.1	76.0	25.6	4.2	136.9
B/D	62.9	N.A.[a]	N.A.[a]	N.A.[a]	62.9
C/D	16.2	67.4	35.9	12.4	131.9
D/E	87.4	84.0	28.5	15.0	214.8
E/F	119.0	52.0	45.3	8.2	224.6
E/G	N.A.[a]	0.2	N.A.[a]	N.A.[a]	0.2
F/G	54.8	34.5	N.A.[a]	3.1	92.3
G/H	50.6	83.7	N.A.[a]	N.A.[a]	134.3
F/I	8.5	N.A.[a]	N.A.[a]	N.A.[a]	8.5
H/I	35.8	36.8	N.A.[a]	N.A.[a]	72.6
I/J	N.A.[a]	101.8	N.A.[a]	N.A.[a]	101.8
Total (km^3)	597.3	703.4	231.7	210.3	1742.8

Notes: Volumes of littoral sand accretion (10^6 m^3) in subaerial beach and dune deposits (≥ 0 m NAVD88) are shown for corresponding timeline intervals (summed polygon cell volumes) for each of the four CRLC subcells. Data are from CentroidData.xls files in Supplementary Data.

[a] N.A. – not applicable, timeline interval does not exist within the sub-cell.

Table 6
Mean shoreline-normalized volume accretion rates in the CRLC subcells.

Interval	Clatsop Plains (m^3 m^{-1} yr^{-1})	Long Beach (m^3 m^{-1} yr^{-1})	Grayland Plains (m^3 m^{-1} yr^{-1})	North Beaches (m^3 m^{-1} yr^{-1})
I/J	–	23.52	–	–
H/I	2.60	2.21	–	–
G/H	2.87	3.34	–	–
F/G	4.96	2.87	0.90	–
E/F	15.05	5.93	7.45	1.65
D/E	5.15	3.12	1.96	1.84
C/D	4.14	4.70	4.80	2.53
B/C	19.53	12.16	6.17	3.13
A/B	0.89	0.80	1.12	0.56
Modern/A	12.49	12.45	10.68	12.38

Notes: Estimated shoreline volume accretion (m^3) between defined timelines (Interval) are normalized for shoreline distance (m^{-1}) and time (yr^{-1}) in the four CRLC subcells to yield mean shoreline-normalized volume accretion rates (m^3 m^{-1} yr^{-1}). Polygon cell sand volumes, as averaged for each of the four CRLC subcells, are from Table 5. Timeline interval age spans are from Table 2. Data are graphically plotted below in Fig. 11.

By comparison, the Long Beach subcell began accretion, at GPR transect PION, with the I/J interval (5.0–4.7 ka), and the Clatsop Plains subcell began accretion, at GPR transect PERK, with the H/I interval (4.7–4.0 ka). Those earliest onset ages of net progradation are associated with positions located next to the mouth of the Columbia River, the source of littoral sand supply to the CRLC system (Fig. 1). But alongshore distances of beach segments from the Columbia River mouth do not entirely account for the different beach-sand volume accretion rates. Though the Grayland Plains subcell is the second most distant subcell from the Columbia River mouth, the highest rate of shoreline-normalized accretion in the C/D interval (4.8 m^3 m^{-1} yr^{-1}) occurred in the Grayland Plains subcell. At the regional scale, the onset ages of shoreline progradation in the CRLC system are likely controlled by competing accommodation space in the inner-shelf (Peterson et al., 2016). But at the subcell scale, both shoreline orientations and estuarine sand sinks played roles in controlling the local shoreline progradations, as discussed below. The origin(s) of the very-small values of shoreline normalized accretion rates in all four subcells during the A/B interval (Fig. 11) remain unknown.

5. Discussion

In this section, the evolutions of the CRLC barriers and beach plains are explained in terms of abundant sand supply from the Columbia River mouth, local shoreline conditions relative to directional wave forcing, and competing accommodation spaces in the large estuarine and inner-shelf sand sinks. Modeling studies of across-shelf transport processes have been completed for other barrier systems (Lorenzo-Trueba and Ashton, 2014; Ortiz and Ashton, 2016), but they differ from those developed for the CRLC system (Sternberg, 1986; Kachel and Smith, 1986), which incorporate both wave dynamics and geostrophic/downwelling or underflow currents to transport littoral sand across the inner-shelf. In this article, the relative importance of the inshore and offshore marine sinks for littoral sand accumulation in the high-wave-energy CRLC system are evaluated empirically for predicted accelerations of future SLR. Estimates of future shoreline retreats are based on the loss of destabilized beach sand to the more competitive marine sand sinks following predicted accelerations of SLR from ongoing global warming.

5.1. Late-Holocene evolution of the barrier and beach plains in the CRLC subcells

The relative timing and magnitude of littoral sand partitioning in the four CRLC subcells (Table 7) are related, in part, to 1) local conditions of shoreline orientations and 2) interceptions of nearshore sand transport by inshore sand sinks in the large marine-dominated estuaries, Willapa Bay and Grays Harbor (Fig. 12). The alongshore limits of late-Holocene littoral sand distribution, or onshore accommodation space, in the CRLC accreted barriers and beach plains are generally controlled by paleo-shoreline orientations. The regional net-northward longshore transport in the CRLC system is reversed in the Clatsop Plains and North Beaches subcells, due to changes in shoreline orientations relative to the west-southwest-west dominant direction of nearshore wave energy. Northwest-southeast trends of latest-prehistoric shorelines located south of 1) the Columbia River delta/spit in the Clatsop Plains subcell (paleo-shoreline bearing 343°TN) and 2) the Point Grenville headland in the North Beaches subcell (350°TN) permit a net southward nearshore transport in those two subcells. The localized southward nearshore transport in the Clatsop Plains subcell is established by Columbia River sand mineralogy in prograded beach plain deposits accreted between the PERK and ESTR transects in the Clatsop Plains subcell (Peterson et al., 2010a). The westward progradation of the Columbia River mouth barrier/delta in late-Holocene time (Fig. 7) promoted southward littoral transport from the Columbia River mouth, yielding the high beach and dune facies accretion rate of 27.4 × 10^6 m^3 ka^{-1} in the Clatsop subcell during late-Holocene time (Table 7). However, the shoreline 'change' to a northeast-southwest orientation (28°TN) between the ESTR profile and Tillamook Head, after 2.5 ka (Peterson et al., 2010c), severely limited littoral sand transport and net deposition, south of the ESR transect in latest-Holocene time.

A net southward onshore/nearshore littoral transport in the North Beaches subcell is indicated by gravel clasts that were eroded from late-Pleistocene deposits in sea cliffs (Vanderburgh et al., 2010), located between Grenville Point and the COPR transect (Fig. 12). The eroded sea cliff gravels were transported south, under traction transport in onshore and nearshore settings, to the Grays Harbor tidal inlet, and rarely, to the southernmost Grayland Plains profile WARR (paleo-shoreline bearing 352°TN), but not further south along the Long Beach Peninsula (2° TN) (Peterson et al., 2010a). A net southward transport of gravel, and presumed accompanying beach sand, in the North Beaches subcell could account, in part, for the modest accretion rates (11.7 × 10^6 m^3 ka^{-1}) in that subcell (Table 7). The apparent southward nearshore/onshore transport in the two northernmost subcells

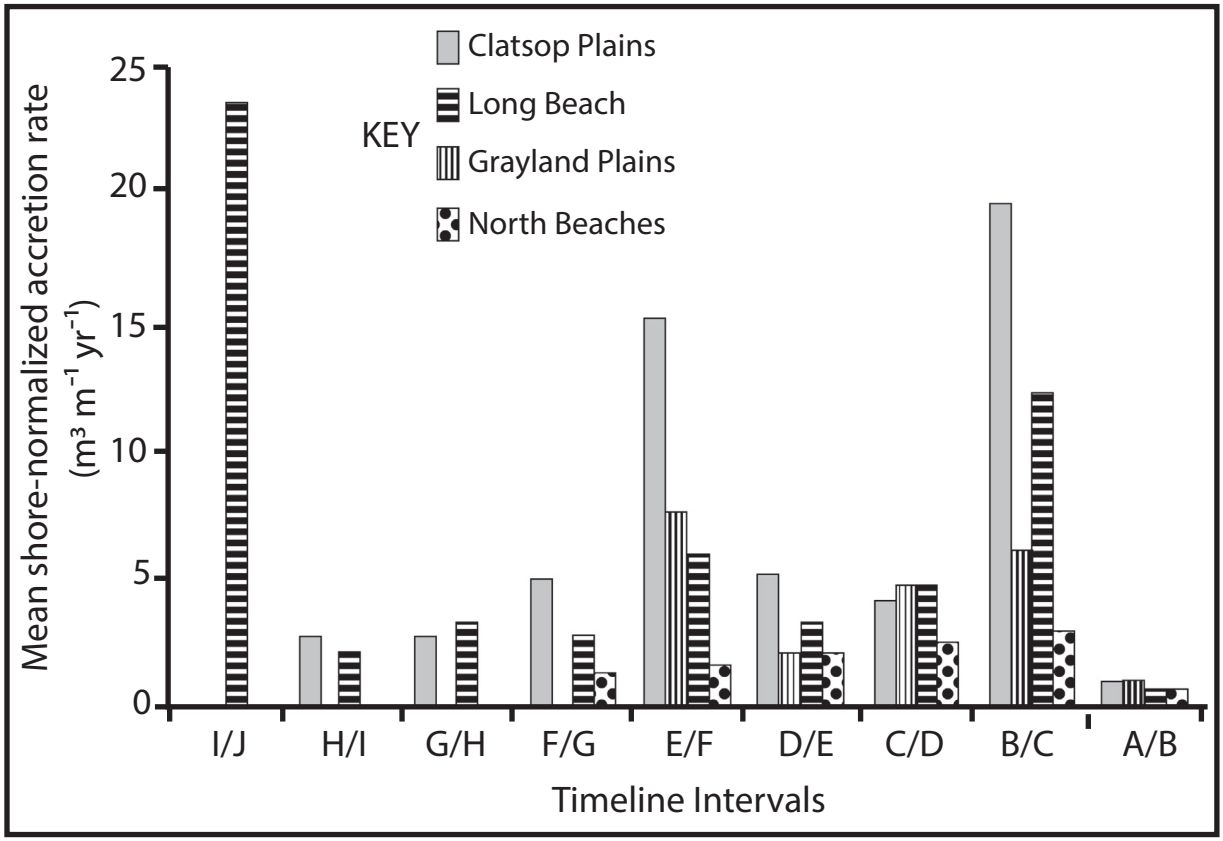

Fig. 11. Mean shoreline-normalized volume accretion rates ($m^3\ m^{-1}\ yr^{-1}$) are plotted for established timeline intervals (paired letters) in the four CRLC subcells. Data are from Table 6. Very-high accretion rates for the I/J interval in the Long Beach subcell are suspect due to uncertain dating of the back-edge of the prograded barrier spit/beach plain.

Table 7
Late-Holocene mean accretion rates for the four CRLC subcell barriers/beach plains and the large marine-dominated estuaries.

Subcell/estuary	Littoral sand volume (m^3)	Onset age of beach accretion (ka)	Mean accretion rate ($\times 10^6\ m^3\ ka^{-1}$)
Clatsop Plains	5.97×10^8	4.7	27.4
Long Beach	7.03×10^8	5.0	19.8
Grayland Plains	2.32×10^8	2.8	15.9
North Beaches	2.10×10^8	2.5	11.7
Willapa Bay estuary	–	–	> 110
Grays Harbor estuary	–	–	117

Notes: Barrier and beach plain sand volume (m^3) includes all intervals from the onset of net accretion to the modern shoreline. Onset age of net accretion is taken to be the earliest polygon cell bounding age or timeline from at least two GPR transects within each subcell. Late-Holocene accretion rates ($m^3\ ka^{-1}$) of littoral sand are the averaged volume accretion rate as normalized to 1000 yr (ka) for all polygon cells within each subcell, since the onset of subcell progradation (Linde, 2014). Measured littoral sand accumulation rates ($m^3\ ka^{-1}$) are also shown for Willapa Bay (Peterson and Vanderburgh, 2018a) and Grays Harbor (Peterson and Vanderburgh, 2018b), as based on the latest-Holocene time period (3–0 ka). Littoral sand accumulation rates in Willapa Bay do not include subtidal channel settings, so the accumulation rate of littoral sand in Willapa Bay is a minimum value.

contrasts with the northward transport of Holocene Columbia River derived sand (hypersthene-rich) in the adjacent inner-shelf, under conditions of orbital wave resuspension and northward geostrophic flow (Peterson et al., 2016).

The large marine-dominated estuaries, Willapa Bay and Grays Harbor, influenced the late onset ages (2–3 ka) of net shoreline progradation in the northern end of the Long Beach subcell, the Grayland Plains subcell, and the north spit of Grays Harbor (Table 7; Fig. 12). Littoral sand accumulation rates in Willapa Bay ($> 110 \times 10^6\ m^3\ ka^{-1}$) and Grays Harbor ($117 \times 10^6\ m^3\ ka^{-1}$) (Peterson and Vanderburgh, 2018a, 2018b) are about one order of magnitude ($10\times$) larger than the corresponding mean accretion rate in the North Beaches subcell ($11.7 \times 10^6\ m^3\ ka^{-1}$), and at least $5\times$ larger than the mean accretion rates in the Grayland subcell ($15.9 \times 10^6\ m^3\ ka^{-1}$) and the Long Beach subcell ($19.8 \times 10^6\ m^3\ ka^{-1}$). As will be addressed later in this article, the competitive roles of these large estuaries for littoral sand accumulations should be significant under conditions of potential future accelerated SLR in the CRLC system.

5.2. Littoral sand accumulation rates in the CRLC inner-shelf during latest-Holocene time

Inner-shelf sand deposits have been vibracored (1–5 m depth subsurface) and ^{14}C dated from sites in the CRLC inner-shelf (Fig. 1) (Kaminsky, 2006), as summarized in Peterson et al. (2016). Bedrock or transgressive gravel deposits occur at the surface in some northernmost inner-shelf localities (Twichell and Cross, 2001; Twichell et al., 2010), which precluded vibracoring in those localities. Sedimentation rates in those settings are based on seismic reflection profiling at identified stations (Peterson et al., 2016). For this article, selected site and core interval data, including subsurface depths and ages, are summarized in a database file ShelfSedRates.pdf, as provided in Supplementary Data. The selected vibracore data are used to establish representative sedimentation rates from the ^{14}C dated vibracore intervals ($n = 56$) in representative core/station sites ($n = 35$) from selected across-shelf transects ($n = 9$) (Fig. 13). Sedimentation rates are computed for sand

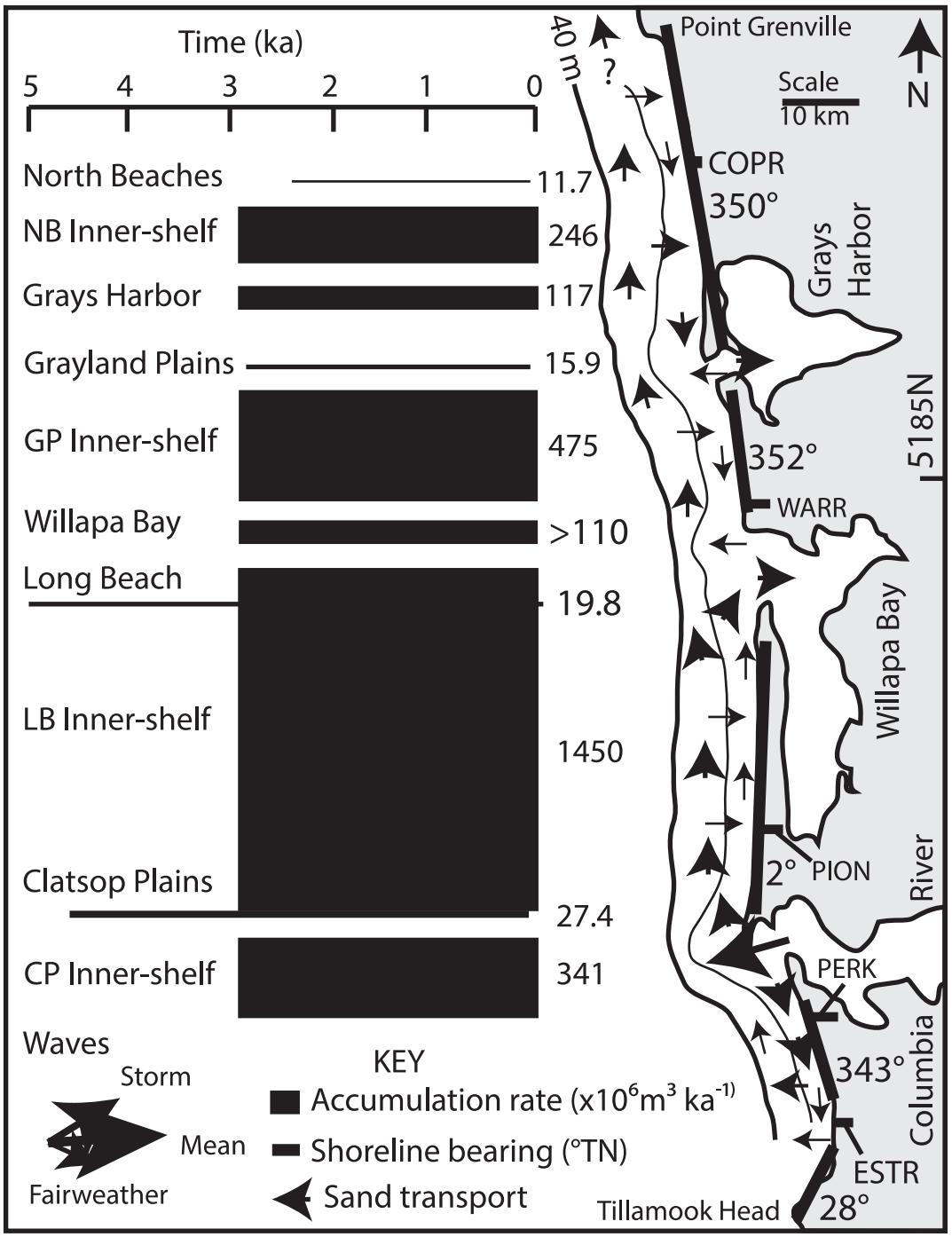

Fig. 12. Littoral sand sinks, as measured by littoral sand accretion or accumulation rates, are shown for 1) the prograded Clatsop Plains, Long Beach barrier, Grayland Plains, and North Beaches, 2) the large marine dominated estuaries, Willapa Bay and Grays Harbor, and 3) the inner-shelf areas (0 m to ~40 m water depth) that correspond to the four CRLC subcells (Fig. 1). Line widths approximate littoral sand accumulation rates (10^6 m^3 ka^{-1}) and line lengths represent the duration of measured accumulation (time line 5–0 ka). Shoreline bearings are shown in degrees true north (°TN). Littoral sand net-transport directions/magnitudes (arrows) are shown for the nearshore and the inner-shelf (bathymetric contours at 20 m intervals). Nearshore dominant wave direction (large arrow) is inferred from beach gravel clast transport. Littoral sand accumulation rates are from Tables 1, 7, and 8.

deposits from ~10 m to 45 m water depths, or from the nearshore to ~10 km distances offshore. Interval sedimentation rates ranged from 11.3 m ka^{-1} in vibracore site LB 306 (31 m water depth) in transect SL33, located just north of the Columbia River ebb tide delta, to 0 m ka^{-1} in all seismic reflection stations (> 8 m water depths) in transects SL7 and SL3, located just south of Point Grenville. The ^{14}C dated vibracore intervals and seismic reflection station sedimentation rates are averaged for each core site, as shown in Fig. 13, and those values are averaged across each transect to yield averaged shelf transect sedimentation rates (Table 8). Averaged shelf-transect sedimentation rates range from 3.41 m ka^{-1} in transect SL33 to 0.17 m ka^{-1} in transect SL3. The vibracore/station transects are also evaluated for

across-shelf gradient, average sand-filled cross-section area per 1000 yr (1 ka), and alongshore length between transect mid-points or subcell boundaries. These data are used to compute the sand-filled volume accumulation rate for each transect during latest-Holocene time

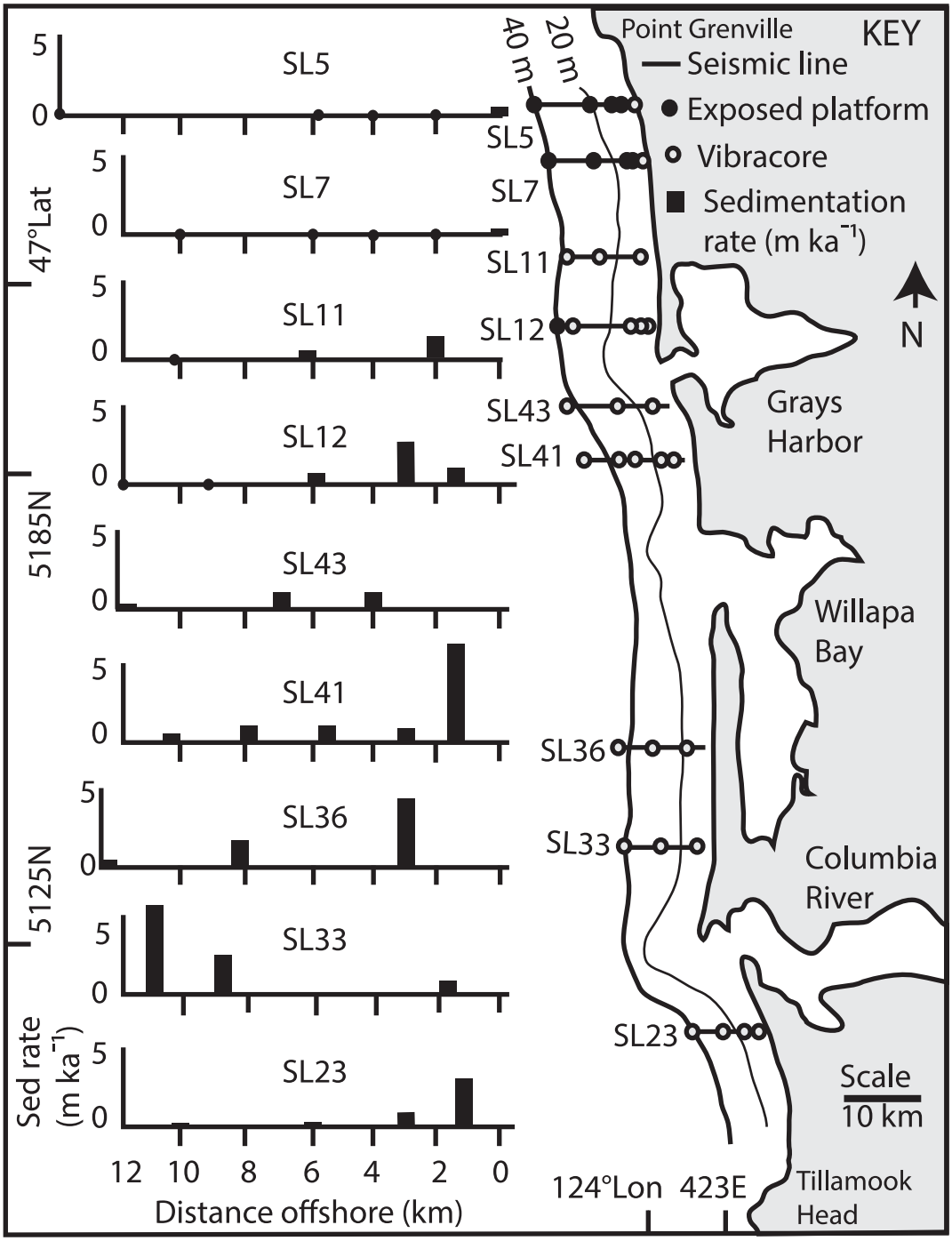

Fig. 13. Inner-shelf seismic lines (SL), wave cut platform sites, as exposed at the surface (solid circles), and offshore vibracore sites (open circles) are shown for the CRLC system. Mean sedimentation rates (m ka^{-1}) for exposed platform sites and vibracores in corresponding inner-shelf seismic line/transects are calculated from Twichell and Cross (2001), Kaminsky (2006), and Peterson et al. (2016). Inner-shelf sediment (sand) thickness and radiocarbon ages are compiled in a summary file ShelfSedRates.pdf, as presented in Supplementary Data. Shelf sand compositions, including percent sand fraction (generally > 90% by weight) and dominant grain size distributions (medium to fine), are provided in Twichell and Cross (2001), Kaminsky (2006), and Peterson et al. (2016). UTM northings are in kilometers.

(3–0 ka).

5.3. Inner-shelf sand sedimentation rates versus across-shelf transect gradients

Mean sedimentation rates from ^{14}C dated vibracore sand intervals (Kaminsky, 2006; as summarized in Peterson et al., 2016) in eight across-shelf transects are plotted against corresponding transect gradients to establish a positive correlation (R^2 = 0.78) during latest-Holocene time (Fig. 14) (ShelfSedRates.pdf in Supplementary Data). The mean sedimentation rate in transect SL33 is excluded from this analysis due to the anomalous high sedimentation rates in its deeper-water sites (31–41 m water depth). Those sites are directly associated with northward littoral sand supply from the adjacent Columbia River ebb tide delta (Fig. 13). The infilling of available accommodation space by abundant littoral sand supply in the inner-shelf eventually decreased the across-shelf gradient in late-Holocene time. The shallowing gradient increasingly favored shoreward sand transport across the inner-shelf,

Table 8
Averaged inner-shelf sedimentation rates and volume accumulation rates.

Transect	Elevation diff. (m)	Distance (m)	Grad. (%)	Sed. rate (m ka^{-1})	Cross-area rate (m^2 ka^{-1})	Length (m)	Acum. rate ($\times 10^6$ m^3 ka^{-1})
SL23	39.5	11,000	0.36	1.07	11,770	29,000	341
SL33	47.6	11,500	0.41	3.41	38,215	22,000	841
SL36	33.6	8500	0.4	2.24	19,040	32,000	609
SL41	44.1	10,800	0.41	2.16	23,328	13,500	319
SL43	47.4	12,500	0.38	0.86	10,750	14,500	156
SL12	43.5	12,100	0.36	1.04	12,584	9500	119
SL11	36.8	10,700	0.34	0.7	7490	7500	562
SL7	40	12,000	0.33	0.22	2640	10,000	264
SL3	40	14,300	0.28	0.17	2431	18,000	437

Notes: Inner-shelf transect data include transect identifications (Twichell and Cross, 2001; Twichell et al., 2010), transect elevation differences (m) and across-shelf distances (m), transect gradient (%), transect averaged sedimentation rate (m ka^{-1}) (ShelfSedRate.pdf in Supplemental Materials), transect cross-sectional area (vertical accretion) rate (m^2 ka^{-1}), transect alongshore length (m) between mid-points or subcell boundaries, and transect volume accumulation rate (x10^6 m^3 ka^{-1}). The transect across-shelf distances and elevation differences are taken from paleo-shoreline positions and elevations at 1.5 ka to the estimated depositional surface at 1.5 ka in the terminal (seawardmost) site. The 1.5 ka inner-shelf transect surface represents the depositional mid-point during latest-Holocene time (3–0 ka).

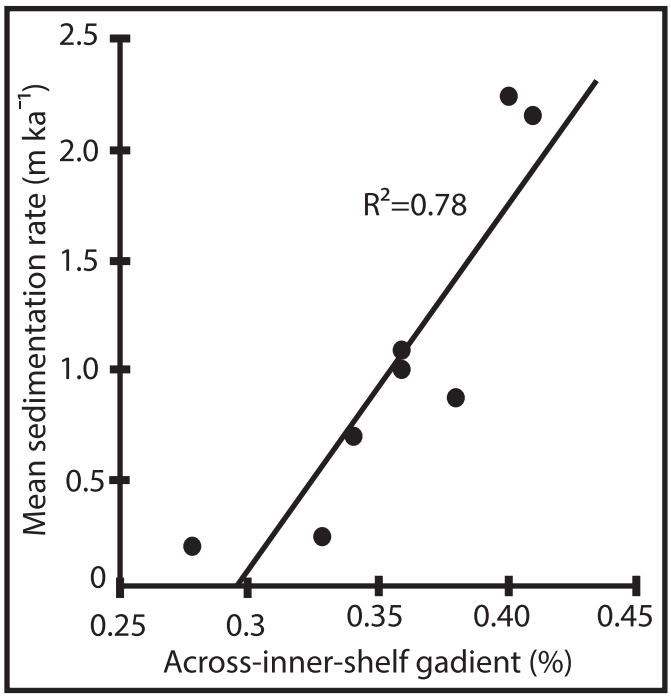

Fig. 14. A plot of mean sedimentation rates (m ka^{-1}) versus across-shelf gradient (%) in corresponding seismic line/vibracore transects in the CRLC system during latest-Holocene time (Fig. 13). Data are from Table 8, excluding vibracores from seismic line SL33, located immediately north of the Columbia River ebb tide delta.

leading to the upper-shoreface progradation in the Clatsop, Long Beach, and Grayland subcells. Nevertheless, inner-shelf gradients exceeding ~0.40% in those subcells are associated with sedimentation rates that continued to keep pace with latest-Holocene rates of net SLR (~1 m ka^{-1}) to offshore distances of at least 8 km or 30 m water depth, as interpreted below (Fig. 13). By comparison, the inner-shelf transect gradients of < 0.35% in the North Beaches subcell generally failed to accumulate significant littoral sand deposits at offshore distances of > 2 km or > 10 m water depth.

Several vibracores in ~45 m water depths (LB304 in SL36, GL504 in SL41 and GL507 in SL43) yield sedimentation rates of 0.32–0.45 m ka^{-1} (ShelfSedRates.pdf in Supplementary Data). These vibracore sites are from representative transects with moderate inner-shelf gradients (0.38–0.41%) in the central subcell areas of the CRLC system (Fig. 13). The long-term sedimentation rates in these deeper water sites fall below the late-Holocene rate of SLR rise (1.0 m ka^{-1}). Vibracores from the same transects, but in shallower water depths of 27–36 m water depth (LB301, GL503, and GL506), demonstrate sedimentation rates (1.1–1.9 m ka^{-1}). These sedimentation rates slightly exceed the rate of late-Holocene SLR. For the central subcells in the CRLC system the long-term (millennial) depth of closure is taken to be between 35 and 40 m water depth during latest-Holocene time. For the purposes of calculating inner-shelf sand accumulation rates following potential near-future SLR (see Section 5.5) a most conservative depth of closure (30 m water depth) is used to represent the offshore extent to which inner-shelf sedimentation rates would match the rate of SLR at the shorter (one century) time scale.

5.4. Offshore, alongshore and onshore transfers of littoral sand in the CRLC system

Columbia River-derived littoral sand likely faced many reversals of alongshore/shelf and across-shore/shelf sand transport in the CRLC system due to 1) variable wave energies and directions at seasonal to inter-decadal (ENSO) time scales (Ruggiero et al., 2005; Ruggiero et al., 2016) and 2) longer-term sea level change reversals at neotectonic cycle time scales (decades to multi-century) (Fig. 2 Part B) (Meyer et al., 1995; Peterson et al., 2010b; Linde, 2014). Nevertheless, a long-term

Table 9
Littoral sand accumulation rates in the CRLC system.

Inner-shelf (subcell area)	Accumulation rate measured ($\times 10^6$ m^3 ka^{-1})	Modified accumulation (sink) from 1.0 m SLR ($\times 10^6$ m^3 m^{-1} SLR)	Total shelf and bay accumulation (sink) from 1.0 m SLR ($\times 10^6$ m^3 m^{-1} SLR)
Clatsop	341	155	155
Long Beach	1450	397	510
Grayland	475	127	240
North Beaches	246	–	
Subtotal	2512	679	
Marine-estuaries			
Willapa Bay	110	110	
Grays Harbor	117	117	
Subtotal	227	227	
Beach/dune			
Clatsop	27.4	–	
Long Beach	19.8	–	
Grayland	15.9	–	
North Beach	11.7	–	
Subtotal	74.8	–	
Grand Total	2814	1002	

Notes: Measured littoral sand accumulation rates that occurred in CRLC subcells during latest-Holocene time are from Tables 7 and 8. Measured littoral sand accumulation rates, in Willapa Bay and Grays Harbor marine-dominated estuaries, from the last 3 ka, are from Peterson and Vanderburgh (2018a, 2018b). Predicted (near-future) subcell offshore accumulations of littoral sand from SLR are based on conversions of measured littoral sand sedimentation rates of 1.0 m ka^{-1} to 1.0 m m^{-1} SLR, based on 1.0 m SLR ka^{-1} (Table 2) in latest-Holocene time. A modified innermost-shelf area of accumulation is taken to be between the nearshore ~10 m water depth, or 2.0 km distrance offshore, and the most conservartive 30 m depth of closure. The total shelf and bay accumulation (sink) includes the modified innermost-shelf area for all three southern subcells, and an addtional 113 $\times$ 10^6 m^3 m^{-1} SLR of littoral sand accumlation each in the Long Beach and Grayland subcells, due to littoral sand sinks in the adjacent estuaries, Willapa Bay and Grays Harbor.

net northward transport in the inner-shelf delivered Holocene Columbia River littoral sand to the northern subcells, where shoreward transport then fed the large marine-dominated estuaries (Willapa Bay and Grays Harbor) and the prograding barriers and beach plains (Fig. 12). The shoreward across-shelf transport was effective in supplying littoral sand to the most distal beaches landward of transects SL5, SL7, SL11, and SL12 in the North Beaches subcell (Fig. 13), due the very shallow gradients of the shelf wave-cut platform (Twichell and Cross, 2001; Twichell et al., 2010). However, a southward onshore/nearshore transport stripped sand from the northernmost beaches, between the Point Grenville and the CORP/SL7 transects, limiting onshore accommodation space there. A southward onshore/nearshore transport also delivered Columbia River-derived littoral sand to the Clatsop subcell, located south of the Columbia River mouth, where net offshore sand transport permitted progradation of the uppermost-submarine shoreface, < 20 m water depth in SL23 (Fig. 13) (Peterson et al., 2010a; Peterson et al., 2016). The net northward transport in the inner-shelf stripped sand from deeper water depths of the Clatsop subcell area (Fig. 11), thereby resulting in the low-sedimentation rates (~0.1 m ka^{-1}) in the deeper submarine shoreface (> 25 m water depth). In the subcells located north of the Columbia River mouth, the northward inner-shelf transport delivered an abundance of Columbia River-derived littoral sand that 1) filled the available inner-shelf accommodation space in middle-Holocene time, and then 2) initiated submarine upper-shoreface progradation in late-Holocene time (Peterson et al., 2016). Subaerial beach and dune facies deposition trailed behind the prograding submarine shoreface deposits. However, local delays in the onset of barrier spit and beach plain progradation until latest-Holocene time (3–0 ka) apparently occurred due to competition for littoral sand with the large marine-dominated estuaries, Willapa Bay and Grays Harbor (Fig. 12). The shallowing inner-shelf gradient in the three southern subcells forced substantial (non-equilibrium) submarine sand accumulation in the uppermost shoreface (Fig. 13) during latest-Holocene time. However, repeated catastrophic shoreline retreat following the last several coseismic subsidence events (Table 2) demonstrated effective beach sand transports offshore to the inner-shelf following the abrupt sea level rises (1–2 m). Whereas the alongshore transport and redistributions of beach sand within, and between, the four subcells were measured at the multi-century time scales (Tables 5 and ShelfSedRates.pdf, as provided in Supplementary Data), the across-shore/shelf transport of beach sand following coseismic subsidence occurred at multi-decade time scales (Fig. 4). The recorded transfers of beach sand from onshore to offshore, following the rapid sea level rises in latest-Holocene time (Table 2), could have occurred at about 10$\times$ the rates of measured alongshore sand redistribution in the CRLC system. The coeval short-term (decadal) sand accumulations in the inner-shelf, following coseismic subsidence, were not resolved in the storm reworked deposits, as ^{14}C dated by Kaminsky (2006).

5.5. Littoral sand accumulations (sinks) in the inner-shelf and the large marine-dominated estuaries

The rates of littoral sand accretion or net storage in the CRLC offshore (inner-shelf) and inshore (large marine-dominated estuaries) are tied to Columbia River sediment supply and to increases in available accommodation spaces. The increases in accommodation space are proportional to the rate of SLR (1.0 m ka^{-1}) in the study area during latest-Holocene time (3–0 ka). However, excessive sedimentation rates (> 1 m ka^{-1}) in the uppermost-submarine shoreface, generally < 20 m water depth (Fig. 13), resulted from upper-shoreface progradation (lateral accretion) in late-Holocene time. As this article is focused on predicted shoreline erosion impacts from future SLR, the lateral shoreface progradation is neglected, but the measured vertical accretion rates (~1.0 m ka^{-1}) in the deeper shoreface settings (20–30 m water depth) are extended across the innermost-shelf to the nearshore (~10 m water depth). As will be shown below in Section 5.6, the nearshore (0–10 m water depth), extending about 2.0 km distance seaward from the modern shoreline, could experience erosion during ravinement, following substantial SLR. For this article the innermost-shelf between the nearshore and the 30 m depth of closure is termed the modified innermost-shelf area of littoral sand accumulation. Due to the narrow beaches and very-low inner-shelf sedimentation rates in the North Beaches subcell area during latest-Holocene time (Fig. 12), that subcell is not included in the computations of predicted innermost-shelf sand accumulation rates following potential future SLR. The modified inner-shelf sand sinks, as estimated for 1.0 m of SLR, over the inner-shelf from the nearshore to 30 m water depth in other three subcells are as follows; 155 $\times$ 10^6 m^3 m^{-1} SLR (Clatsop Plains), 397 $\times$ 10^6 m^3 m^{-1} SLR (Long Beach), 127 $\times$ 10^6 m^3 m^{-1} SLR (Grayland Plains), as shown in Table 9.

Could new river sand, as potentially supplied to the littoral system from the large Columbia River, offset some littoral sand loss to the large marine sand sinks in the inner-shelf and marine dominated estuaries? Littoral sand throughput from the Columbia River is estimated to have been at least 2814 $\times$ 10^6 m^3 ka^{-1} during late-Holocene time, as based on the summing of littoral sand sinks in the inner-shelf and marine-dominated estuaries, Willapa Bay and Grays Harbor (Table 9). This value is smaller than that of 3720 $\times$ 10^6 m^3 ka^{-1}, as based on longer early- to late-Holocene time intervals measured for the inner-shelf and Grays Harbor (Table 1). The current throughput of Columbia River sand is not known relative to prehistoric conditions, due the lack of sand retention measurements in numerous impoundments (> 100 in number) in the Columbia River tributaries. However, a modeled historic throughput value of 2.7 $\times$ 10^6 m^3 yr^{-1} has been proposed by Kaminsky et al. (2001). The estimated supplies of Columbia River sand

to the CRLC inner-shelf, estuary, and barrier/beach plain sinks are relatively similar for Holocene time (~3.7 × 10^6 m^3 yr^{-1}) and latest-Holocene time (~2.8 × 10^6 m^3 ka^{-1}). Some sand loss occurred from lithic fragment abrasion in the surf zone (~30%) and sand transport north out of CRLC system (Peterson et al., 2016). Given those losses the averaged sand sink accumulation rates ~3.3 × 10^6 m^3 ka^{-1}, are not substantially different from the previously reported Columbia River bed load throughput rates of about 5 × 10^6 m^3 ka^{-1}, as based on time-varying bed load fill rates in the Columbia River estuary (Peterson et al., 2013). The estimated sand budgets in the CRLC system are relatively well-balanced throughout middle- to late-Holocene time.

For the purposes of predicting potential shoreline response to SLR is this article, we assume a hypothetical Columbia River sand throughput value of 3 × 10^6 m^3 yr^{-1}, which translates into 300 × 10^6 m^3 per 100 yr or 600 × 10^6 m^3 per 200 yr. In either case, most of the hypothetical new river sand supply (300–600 million cubic meters over one to two centuries) would not reach the estuary mouth due to increasing accommodation in the estuary following an accelerated SLR. For example, during late-Holocene time the bedload (sand) accommodation space in the Columbia River was 570 × 10^6 m^3 ka^{-1} (Peterson et al., 2013) or 570 × 10^6 m^{-1} SLR, assuming a late-Holocene SLR of 1.0 m ka^{-1} (Fig. 2 Part A). The projected increase in accommodation space, due to potential SLR of 1–3 m, is similar in volume to the hypothetical Columbia River sand production over a 1–2 century time interval. Therefore, sand in-filling of increasing accommodation space in the Columbia River estuary would largely cancel-out the potential river sand throughput to the littoral zone from a 1–3 m SLR during the next century or two. Such infilling of bedload accommodation space by new Columbia River sand would also largely preclude reentry of littoral (beach) sand back into the lower Columbia River estuary reaches, following a near-future SLR of ≤3 m.

5.6. Predicted shoreline retreat following potential future sea level rise

In this article, subcell averaged shoreline retreat distances are based on onshore sand volume loss to increasing marine accommodation space, following potential near-future SLR values of 1–3 m. Offshore (seaward) sand transport in the CRLC system by wave oscillatory currents, geostrophic flow and down-welling, has been modeled by Kachel and Smith (1986). Such offshore transport and dispersal of Columbia River sand, as modeled by Sternberg (1986) and Kachel and Smith (1986), are directly confirmed by shelf littoral sand sedimentation rates, as summarized here in Table 8. The accommodation space mechanisms of littoral sand transport into and retention in the large marine-dominated estuaries are discussed elsewhere for Willapa Bay and Grays Harbor (Peterson and Vanderburgh, 2018a, 2018b). The major marine sinks of littoral sand occur in the innermost-shelf (total = 679 × 10^6 m^3 m^{-1} SLR) (Table 9). However, the large marine-dominated estuaries, Willapa Bay and Grays Harbor, are also significant sinks (total = 227 × 10^6 m^3 m^{-1} SLR). For this article, the littoral sand sinks in Willapa Bay and Grays Harbor estuaries are split between the Long Beach and Grayland Plains subcells to yield combined marine sinks of littoral sand for the Long Beach and Grayland Plains subcells. No littoral sand is assumed to be lost or gained from the Clatsop subcell to the Columbia River estuary during the near future period (1–2 centuries) of potential SLR (1–3 m), as previously discussed in Section 5.5. For the purposes of this article, the potential sand transfers from onshore to offshore are taken to occur within corresponding subcell areas of the Clatsop, Long Beach and Grayland subcells. Sand volume loss or gain between the four CRLC subcells could be addressed in future studies by combining the marine sinks and averaging the shoreline sand loss proportionally across the four subcells on bases of identified longshore transport parameters.

The predicted subcell beach sand losses to increasing offshore/inshore marine accommodation spaces from SLR are used here to estimate corresponding shoreline retreat distances (Fig. 15). Specifically, the onshore (subaerial) eroded sand volumes for different timeline intervals (Table 5) are added to submarine eroded sand volumes (< 0 m NAVD88) to yield a total sand volume loss for the analyzed subcells. The onshore submarine eroded sand volume is calculated from translating the modern nearshore gradient (1.0%) landward. An equal volume is assumed for the nearshore eroded sand volume. Both distances of submarine eroded sand volumes are scaled to the distance of onshore retreat. The cross-sectional areas of submarine erosion are multiplied by the subcell inner-shelf length to yield the subcell submarine erosion volume. The subaerial erosion volume between timelines, and corresponding submarine erosion volumes, are combined to yield the subcell total erosion volume. That is the subcell erosion volume needed to fill the subcell increased accommodation spaces corresponding to potential future SLR. Because no post-submergence accumulation is assumed for the eroded nearshore, ~2.0 km width estimated for 2 m SLR (as shown in Fig. 15), that area is excluded from the inner-shelf accommodation space. The relations above are compared to find the closest match between the subcell increased submarine accommodation space and the total subcell erosion volume, corresponding to the different onshore timeline intervals (Table 10). The closest matches yield subcell averaged retreat distances for potential for SLR of 1.0 m, 2.0 m and 3.0 m in the CRLC system (Fig. 16). Predicted averaged shoreline retreat distances for 2.0 m of SLR are as follows; ~0.7 km (Clatsop Plains subcell), ~1.2 km (Long Beach subcell), and ~1.3 km (Grayland Plains subcell).

The averaged retreat distances (Table 10) are reported to 0.1 km resolution, but they could be under-estimated by as much as 30%. These retreat estimates are assumed to be minimum values for assumed SLR for the following reasons 1) the subtidal area of littoral sand accumulation in Willapa Bay (40% of Willapa Bay surface area or about 25% of the total Willapa Bay and Grays Harbor surface area) is not included in the estuarine littoral sand sinks (Table 9) and 2) the outermost inner-shelf areas (30–50 m water depth) are not included in the inner-shelf sand sinks, as they might not accumulate littoral sand at the rate of near-future SLR. The outermost inner-shelf deposits account for less than 20% of the total inner-shelf littoral sand accumulations during late-Holocene time (ShelfSedRates.pdf in Supplementary Data). Submarine littoral sink errors (inner-shelf and estuaries), as based on surface area uncertainties, could reach 30% (mostly under-estimated). However, the largest uncertainties in shoreline retreat distances arise from the amounts of SLR, posed here, as scenarios of 1.0 m, 2.0 m, and 3.0 m. The corresponding accumulation thicknesses of littoral sand yield uncertainties of vertical accretion, reaching up to 300%. Given assumed SLR values, and corresponding littoral sand thicknesses for the different scenarios, the estimated averaged retreat distances could vary by 30% for each scenario. Site specific uncertainties could be greater due to local variations from the mean conditions.

Averaged shoreline retreat values, as predicted by the volume accommodation space relations presented in this article (Table 10), are compared to shoreline retreat distances that were predicted by the modified Bruun method (Bruun, 1962; Komar et al., 1991), as utilized for the CRLC beaches by Doyle (1996). The simplified Bruun method parameters used by Doyle (1996) are; 1) across-shore beach retreat (R), 2) measured modern mid-beach berm heights (B = 3–4 m), 3) potential SLR rise (S = 2.0 m), 4) offshore interdecadal depths of closure (h = 20 m), and 5) offshore distances (L) to the point of depth of closure, where R = S{L/(B + h)}. Representative profiles analyzed by Doyle (1996) totaled n = 6 in the Clatsop subcell, n = 6 in the Long Beach subcell, and n = 3 in the Grayland subcell. Averaged retreat distances from 2.0 m of SLR are 300 m, 400 m and 400 m, respectively, for the Clatsop Plains, Long Beach, and Grayland Plains subcells. Those retreat distances (Doyle, 1996) are only ~30–50% as large as those estimated by the measured accommodation relations as used in this article (Table 10). The differences between the two approaches are attributed to 1) the greater across-shelf distances of net sand accumulation assumed for the 1–2 century time scales and 2) the large marine-dominated estuarine sand sinks (Willapa Bay and Grays Harbor) that

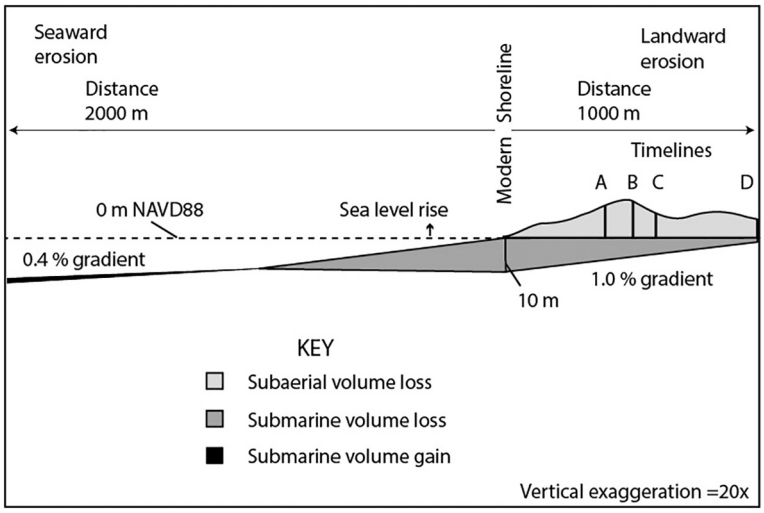

Fig. 15. Diagram of onshore and nearshore sand volume losses for a hypothetical retreat interval (A-D), including subaerial eroded volumes (lightly shaded) and submarine eroded volumes (darkly shaded) from a 2 m SLR in the Long Beach subcell. Some accumulation is shown for the seaward portion of the submarine nearshore, but the transition zone to 2.0 km seaward of the present shoreline is not included in marine sink sand accumulation estimates. This transition zone (1/3 of the innermost-shelf profile distance) is assumed from equilibrium profile shifts (Bruun, 1962). The depth of truncation is based on a 1.0% ravinement gradient and distance from the maximum retreat or timeline 'D'. The onshore eroded basal slope (1.0% gradient) is translated (shifted) landward from the modern nearshore gradient. The modern nearshore gradient (1.0%) is taken from the modern beach toe (0 m NAVD88) to 1.0 km distance offshore in transects from the Clatsop, Long Beach, and Grayland subcells. The 0 m NAVD88 elevation datum is ~1.0 m below mean sea level (MSL) in the study area. Diagram vertical exaggeration is 20×.

Table 10
Shoreline volume loss and retreat distance.

Subcell/ SLR (m)	Total marine sink volume ($\times 10^6$ m^3)	Onshore timeline interval	Eroded subaerial volume ($\times 10^6$ m^3)	Eroded submarine volume ($\times 10^6$ m^3)	Eroded combined volume ($\times 10^6$ m^3)	Averaged retreat distance (km)
Clatsop						
1.0	155	Mod/A	110	30	140	0.3
2.0	310	Mod/C	160	120	280	0.7
3.0	465	Mod/D	240	390	640	1.2
Long Beach						
1.0	510	Mod/B	170	310	470	0.7
2.0	1020	Mod/D	310	800	1110	1.1
3.0	1530	Mod/E	390	1230	1620	1.5
Grayland						
1.0	240	Mod/A	80	120	190	0.7
2.0	480	Mod/B	100	360	460	1.3
3.0	720	Mod/D	160	520	670	1.5

Notes: The total retreat volumes (subaerial and submarine) (x10^6 m^3) are established for each subcell onshore timeline interval. The submarine sand sinks include both the inner-self (all three subcells) and the large marine-dominated estuaries, Willapa Bay (Long Beach subcell) and Grays Harbor (split between the Long Beach and Grayland Plains subcells). The closest combined eroded volume for each subcell is then found for the predicted total marine sink for a given SLR value (1, 2, or 3 m). The matched timeline intervals yield the subcell averaged retreat distances (m). Averaged retreat distances are reported to 0.1 km (resolution) but they have estimated uncertainties of as much as 30%.

are included in the measured accommodation space relations. Ranasinghe et al. (2012) also reported much larger beach retreat values in some settings, relative to the simple Bruun Method, due to sediment sinks in tidal inlets. The measured accommodation space approach proposed in this article, offers advantages in that shoreline susceptibility to future SLR can be evaluated relative to measured values of sand supply and sand loss, as calibrated to past conditions of sea level change. The measured accommodation space relations demonstrated in this article were found to be particularly applicable to the complex and interactive settings in the large CRLC system. Such approaches are recommended for other similarly-complex littoral systems worldwide.

6. Conclusion

In complex littoral systems, such as the Columbia River Littoral Cell (CRLC), accommodation spaces in different depositional environments, such as the inner-shelf, estuaries, and beaches can be thought of as competing for available littoral sand supply. Some accommodation spaces fill before others, leading to predictable sequences of coastal evolution. Under conditions of littoral sediment deficit or when new submarine accommodation space is added, such as during sea level rise (SLR), it is expected that the onshore accommodation spaces, last to fill, will be the first to empty, leading to predicted sequences of beach erosion. In this article, the depositional evolutions of the prograded barriers and beach plains in the CRLC system are explained in terms of sequential filling of available accommodation spaces in different depositional environments and in different shoreline segments during late-Holocene time. Filling of the inner-shelf and the large marine-dominated estuaries, Grays Harbor and Willapa Bay, preceded upper-shoreface progradation and accretion of subaerial beach and foredune deposits in the Long Beach, Clatsop Plains, Grayland Plains, and North Beaches subcells. Overlap of accommodation space filling in the innershelf and estuaries has continued into late-Holocene time. However, measured accumulation rates decrease in magnitude from the inner-shelf to the large marine-dominated estuaries to the onshore beach segments in the four CRLC subcell areas.

The order of accommodation space filling is hypothetically 'reversed' to predict shoreline retreat in the four CRLC subcells following potential SLR from ongoing global warming. The subcell beaches and barriers will be eroded to fill increasing accommodation space in the inner-shelf and in the large marine-dominated estuaries. The high energies of waves, tides, and onshore-winds in the CRLC system permitted the barrier and beach plain shorelines and large marine-dominated estuaries to respond to episodic coseismic subsidence and interseismic uplift, over time scales of several decades. In such high-energy littoral systems, the shoreline erosion response to potential future accelerated SLR is expected to 'keep pace' with the predicted rates of potential eustatic sea level rise (1–3 m) over the next 100–200 years. Beach sand losses to increasing offshore (inner-shelf) and inshore (estuary) submarine accommodation spaces in the CRLC system, resulting from near future SLR of 2.0 m, are estimated to result in shoreline retreat distances of 0.7–1.3 km, representing 25–50% of the widths of prograded barrier spits and beach plains. The severe beach retreat estimates reported here are due to the wide-scale transfers of beach sand to increasing submarine accommodation spaces in the inner-shelf and in large marine-dominated estuaries, following potential future SLR. Such severe beach retreat estimates, as predicted for the CRLC system, should serve as warnings about future catastrophic beach erosion resulting from near-future SLR in other high-wave-energy sandy shorelines worldwide.

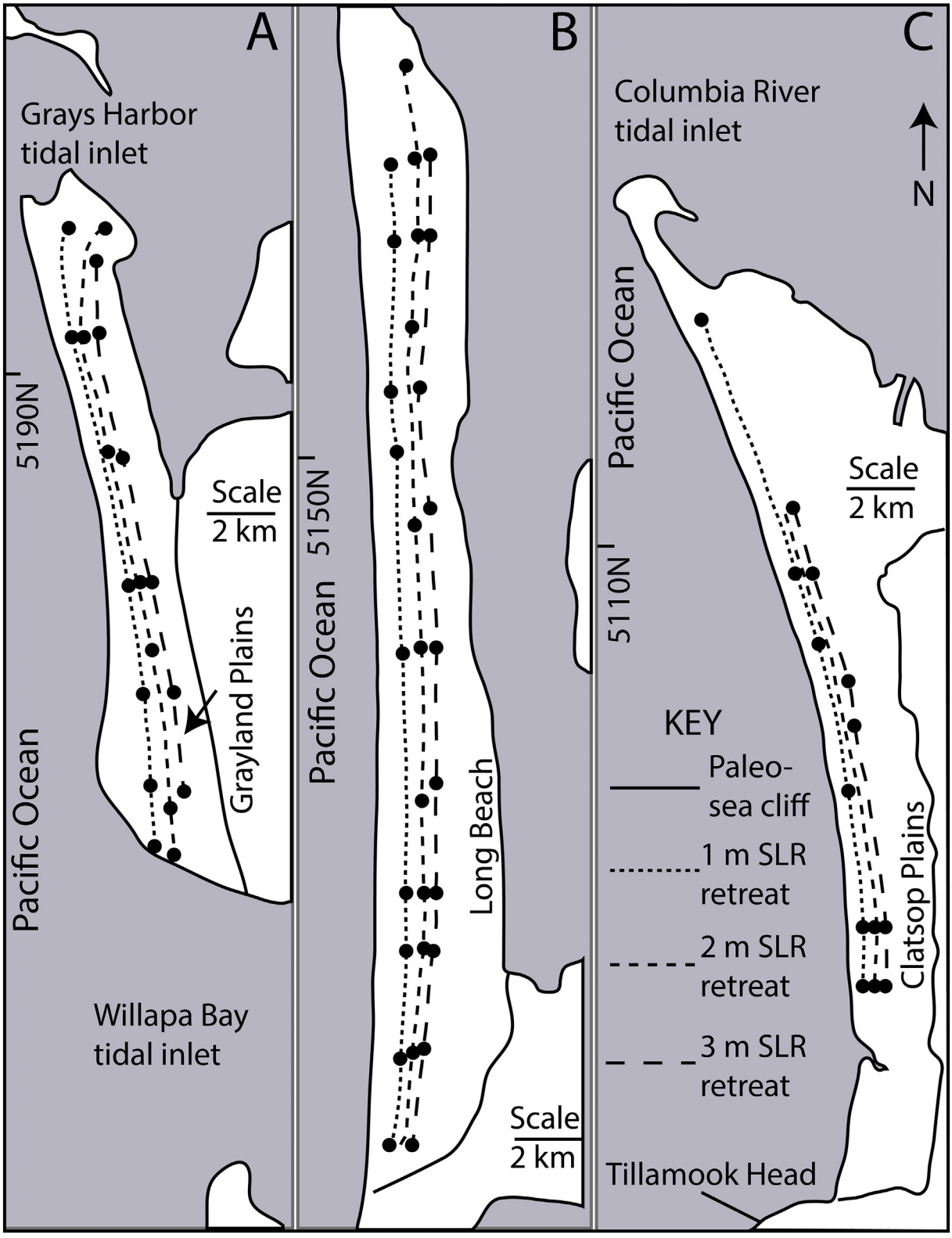

Fig. 16. Predicted shoreline erosion from beach sand transfer to offshore (inner-shelf) and inshore (marine dominated estuaries) following predicted near-future SLR at 1 m, 2 m, and 3 m. Data are from Table 10. Landward centroid positions used to map retreat interval distances are shown (solid circles). Retreat lines (dashed) between identified centroids are guided by abandoned foredunes, as used to constrain polygon cell boundaries (Figs. 7 and 8). Predicted local retreat line positions (solid circles) are shown to 0.4 km resolution or 30% of a representative retreat distance of 1.3 km for 2–3 m SLR. UTM northing coordinates are in kilometers. See Fig. 1 for subcell locations in the CRLC system.

Declaration of Competing Interest

The authors declare that they have no known competing financial interests or personal relationships that could have appeared to influence the work reported in this paper.

Acknowledgements

Prehistoric sediment budget analyses and accommodation space applications in the Columbia River Littoral Cell (CRLC) system were initially encouraged by James Phipps, Kenneth Scheidegger, Larry Sloss, Chris Kraft, Jerry Glenn, and Derald Smith. Graduate student thesis studies to help support these analyses have been performed by Edward Gates, Lorraine Woxell, April Herb, Diana Baker, and George Kaminsky. Kenneth Cruikshank assisted with database design for the CRLC prograded barrier spits and beach plains in this article. Marie Ferland assisted with vibracoring, core logging, and radiocarbon sampling, in the CRLC inner-shelf. Kennett Peterson assisted with editing early versions of this article. This work was funded, in part, by the U.S. Geological Survey, Coastal and Marine Geology Program, under the South West Washington Coastal Erosion Project, Coop #1434-HQ-96-AG-01612 from 1996 to 2001. Additional funding (2001 to present) has been provided by Fraser Valley College, Lethbridge College, Medicine Hat College, and Kwantlen Polytechnic University.

References

Alder, J.R., Hostetler, S.W., 2015. Global climate simulations at 3000-year intervals for the last 21,000 years with the GENMOM coupled atmosphere-ocean model. Clim. Past 11, 449–471.
Atwater, B.F., Hemphill-Haley, E., 1997. Recurrence intervals for great earthquakes of the past 3,500 years at northeastern Willapa Bay, Washington. In: US Geological Survey Professional Paper 1576, (1–108 p).
Atwater, B.F., Tuttle, M.P., Schweig, E.S., Rubin, C.M., Yamaguchi, D.K., Hemphill-Haley, E., 2004. Earthquake recurrence, inferred from paleoseismology. In: Gillespie, A.R., Porter, S.C., Atwater, B.F. (Eds.), The Quaternary Period in the United States. Elsevier, Amsterdam, pp. 331–350.
Baker, D., Peterson, C., Hemphill-Haley, E., Twichel, D., 2010. Holocene sedimentation in the Columbia River Estuary. Mar. Geol. 273, 83–95.
Bamber, J.L., Oppenheimer, M., Kopp, R.E., Aspinall, W.P., Cooke, R.M., 2019. Ice sheet contributions to future sea-level rise from structured expert judgment. Proc. Natl. Acad. Sci. 116, 11195–11200.
Bruun, P., 1962. Sea-level rise as a cause of shore erosion. J. Waterways Harbors Div. 88, 117–132.
Calib7.10, 2019. Radiocarbon Calibration Program. CALIB REV7.1.0. http://calib.org/calib/calib.html (Accessed May 25, 2019).
Cruikshank, K.M., Peterson, C.D., 2017. Late-stage interseismic strain interval, Cascadia subduction zone margin, USA and Canada. Open J. Earthq. Res. 6, 1–34.
Darienzo, M.E., Peterson, C.D., Clough, C., 1994. Stratigraphic evidence for great subduction zone earthquakes at four estuaries in Northern Oregon. J. Coast. Res. 10, 850–876.
DeConto, R.M., Pollard, D., 2016. Contribution of Antarctica to past and future sea-level rise. Nature 531, 591–597.
Doyle, D.L., 1996. Beach Response to Subsidence Following a Cascadia Subduction Zone Earthquake along the Washington-Oregon Coast. M.S. Thesis, Portland State University, Portland, Oregon (113 p).
Gesch, D., Oimoen, M., Greenlee, S., Nelson, C., Steuck, M., Tyler, D., 2002. The National Elevation Dataset: Photogrammetric Engineering and Remote Sensing. 68. pp. 5–32.
Herb, A.A., 2000. Holocene Stratigraphy and Sediment Volumes for the Columbia River Littoral Cell, Pacific Northwest, USA. M.S. Thesis, Portland State University, Portland, Oregon (186 p).
Jevrejeva, S., Moore, J.C., Grinsted, A., 2012. Sea level projections to AD2500 with a new generation of climate change scenarios. Glob. Planet. Chang. 80, 14–20.
Jol, H.M., Peterson, C.D., Vanderburgh, S., Phipps, J., 1999. GPR as a regional geomorphic tool: shoreline accretion/erosion along the Columbia River littoral cell. In: Proceedings of the Seventh International Conference on Ground Penetrating Radar (GPR'98). vol. 1. University of Kansas, Lawrence, Kansas, pp. 257–262.
Jol, H.M., Lawton, D.C., Smith, D.G., 2003. Ground penetrating radar: 2-D and 3-D subsurface imaging of a coastal barrier spit, Long Beach, WA, USA. Geomorphology 53, 165–181.
Jurney, C., 2001. Refining the Measured Frequency of Great Earthquakes along the Cascadia Subduction Zone. M.S. thesis, Central Washington University, Ellensberg, Washington (78 p).
Kachel, N.B., Smith, J.D., 1986. Geologic impact of sediment transporting events on the Washington continental shelf. In: Knight, R.J., McLean, J.R. (Eds.), Shelf Sands and Sandstones. Canadian Society of Petroleum Geologists, Memoir II, pp. 145–162.
Kaminsky, G.M., 2006. Shoreface Behavior and Equilibrium. Unpublished PhD Thesis. University of Sydney, New South Wales (633 p).
Kaminsky, G.M., Buijsman, M.C., Ruggiero, P., 2001. Predicting shoreline change at decadal scale in the Pacific Northwest, USA. In: Proceedings of the 27th International Conference on Coastal Engineering. American Society of Civil Engineers, pp. 2400–2413.
Kaminsky, G.M., Ruggiero, Buijsman, M.C., McCandless, D., Gelfenbaum, G., 2010. Historical evolution of the Columbia River littoral cell. Mar. Geol. 273, 96–126.
Komar, P.D., Lanfredi, N., Baba, M., Dean, R.G., Dyer, K., Healy, T., Ibe, A.C., Terwindt, J.H.J., Thom, B.G., 1991. The response of beaches to sea-level changes-a review of predictive models. J. Coast. Res. 7, 895–921.
Kopp, R.E., Horton, R.M., Little, C.M., Mitrovica, J.X., Oppenheimer, M., Rasmussen, D.J., Strauss, B.H., Tebaldi, C., 2014. Probabilistic 21st and 22nd century sea-level projections at a global network of tide-gauge sites. Earth's Future 2, 383–406.
Kopp, R.E., Gilmore, E.A., Little, C.M., Lorenzo-Trueba, J., Ramenzoni, V.C., Sweet, W.V., 2019. AGU Centennial Grand Challenge: Sea-level science on the frontier of usability. Earth's Future. AGU Adv. Earth Space Sci. 7, 1235–1269.
Linde, T., 2014. Regional Database Analysis of Dated Prehistoric Shorelines to Establish Sand Partitioning in Late Holocene Barriers and Beach Plains of the Columbia River Littoral Cell, Washington and Oregon, USA. M.S. Thesis. Portland State University, Oregon (86 p).
Lorenzo-Trueba, J., Ashton, A.D., 2014. Rollover, drowning, and discontinuous retreat: Distinct modes of barrier response to sea-level rise arising from a simple morphodynamic model. J. Geophys. Res. Earth Surf. Process. 119, 779–801.
Mengel, M., Levermann, A., Frieler, K., Robinson, A., Marzeion, B., Winkelmann, R., 2016. Future Sea level rise constrained by observations and long-term commitment. Proc. Natl. Acad. Sci. 113, 2597–2602.
Meyers, R.A., Smith, D.G., Jol, H.M., Peterson, C.D., 1996. Evidence for eight great earthquake-subsidence events detected with ground-penetrating radar, Willapa barrier, Washington. Geology 24, 99–102.
Ortiz, A.C., Ashton, A.D., 2016. Exploring shoreface dynamics and a mechanistic explanation for a morphodynamic depth of closure. J. Geophys. Res. Earth Surf. Process. 121, 442–464.
Peterson, C.D., Cruikshank, K.M., 2014. Quaternary tectonic deformation, Holocene paleoseismicity, and modern strain in the unusually-wide coupled zone of the central Cascadia margin, Washington and Oregon, USA and British Columbia, Canada. J. Geogr. Geol. 6 (33 p).
Peterson, C.D., Phipps, J.B., 2016. Accommodation space controls on incised-valley sediment accumulation rates during the Holocene marine transgression (0–11 ka) in Grays Harbor, a large meso-tidal estuary, Washington, USA. Mar. Geol. 380, 1–16.
Peterson, C.D., Vanderburgh, S., 2018a. Tidal flat depositional response to neotectonic cyclic uplift and subsidence (1–2 m) as superimposed on latest-Holocene net sea level rise (1.0 m/ka) in a large shallow mesotidal wave-dominated estuary, Willapa Bay, Washington, USA. J. Geogr. Geol. 10, 109–139.
Peterson, C.D., Vanderburgh, S., 2018b. Interconnected accommodation space controls between sand-charged shallow tidal channels and wind-wave truncated tidal flats during latest-Holocene Sea level rise (~3.0 m) in a large mesotidal wave-dominated estuary, Grays Harbor, Washington, USA. J. Geogr. Geol. 10, 26–56.
Peterson, C.D., Doyle, D.L., Barnett, E.T., 2000. Coastal flooding and beach retreat from coseismic subsidence in the Central Cascadia margin, USA. Environ. Eng. Geol. 6, 255–269.
Peterson, C.D., Vanderburgh, S., Roberts, M.C., Jol, H.M., Phipps, J.P., Twichell, D.C., 2010a. Composition, age, and depositional rates of Holocene shoreface deposits under barriers and beach plains of the Columbia River littoral cell, USA. Mar. Geol. 273, 62–82.
Peterson, C.D., Jol, H.M., Vanderburgh, S., Phipps, J.B., Percy, D., Gelfenbaum, G., 2010b. Dating of late-Holocene shoreline positions by regional correlation of coseismic retreat events in the Columbia River littoral cell. Mar. Geol. 273, 44–61.
Peterson, C.D., Jol, H.M., Horning, T., Cruikshank, K.M., 2010c. Paleotsunami Inundation of a Beach Ridge Plain: Cobble Ridge Overtopping and Inter-ridge Valley Flooding in Seaside, Oregon, USA. J. Geol. Res (22 p. Article ID 276989).
Peterson, C.D., Gates, E.B., Minor, R., Baker, D.L., 2013. Accommodation space controls on the latest Pleistocene and Holocene (16-0 ka) sediment size and bypassing in the lower Columbia River Valley: a large fluvial-tidal system in Oregon and Washington, USA. J. Coast. Res. 29, 1191–1211.
Peterson, C.D., Vanderburgh, S., Roberts, M., 2014. Late Holocene Geomorphology of the Columbia River Estuary, Oregon and Washington, USA. J. Geogr. Geol. 6, 1–27.
Peterson, C.D., Twichell, D.C., Roberts, M.C., Vanderburgh, S., Hostetler, S.W., 2016. Accommodation space in a high-wave-energy inner-shelf during the Holocene marine transgression: correlation of onshore and offshore inner-shelf deposits (0-12 ka) in the Columbia River littoral cell system, Washington and Oregon, USA. Mar. Geol. 379, 140–156.
Phipps, J., Jol, H.M., Peterson, C.D., Vanderburgh, S., 2001. Sand dune reactivation and subduction zone earthquakes in the Grayland area. Wash. Geol. 28, 31–33.
Ranasinghe, R.T., Duong, M., Uhlenbrook, S., Roelvink, D., Stive, M.J.F., 2012. Climate-change impact assessment for inlet-interrupted coastlines. Nat. Clim. Chang. 3, 83–87.
Rankin, D.K., 1983. Holocene Geologic History of the Clatsop Plains Foredune Ridge Complex. M.S. Thesis. Portland State University, Portland, Oregon (175 p).
Reckendorf, F., Peterson, C., Percy, D., 2001. The Dune Ridges of Clatsop County, Oregon. State of Oregon Department of Geology and Mineral Resources, Open-File Report O-01-07, CDRom.
Ruggiero, P., Kaminsky, G.W., Komar, P.D., McDougal, W.G., 1997. Extreme waves and coastal erosion in the Pacific Northwest. In: Proceedings of Waves '97 ASCE, pp. 947–961.
Ruggiero, P., Kaminsky, G.M., Gelfenbaum, G., Voigt, B., 2005. Seasonal to interannual morphodynamics along a high-energy dissipative littoral cell. J. Coast. Res. 553–578.

Ruggiero, P., Kaminsky, G.M., Gelfenbaum, G., Cohn, N., 2016. Morphodynamics of prograding beaches: a synthesis of seasonal-to century-scale observations of the Columbia River littoral cell. Mar. Geol. 376, 51–68.
Satake, K., Shimazaki, K., Tsuji, Y., Ueda, K., 1996. Time and size of giant earthquake in Cascadia inferred from Japanese tsunami records of January 1700. Nature 378, 246–249.
Schlichting, R.B., Peterson, C.D., 2006. Mapped Overland Distance of paleotsunami high-velocity inundation in back-barrier wetlands of the Central Cascadia margin, USA. J. Geol. 114, 577–592.
Sherwood, C.R., Jay, D.A., Harvey, B., Hamilton, P., Simenstad, C.A., 1990. Historical changes in the Columbia River estuary. Prog. Oceanogr. 25, 299–352.
Sternberg, R.W., 1986. Transport and accumulation of river-derived sediment on the Washington continental shelf, USA. J. Geol. Soc. Lond. 143, 945–956.
Twichell, D.C., Cross, V.A., 2001. Holocene evolution of the southern Washington and northern Oregon shelf and coast: Geologic discussion and GIS data release. In: U.S. Geological Survey, Open File Report 01–076, (27 p., and CDRom disk).
Twichell, D.C., Cross, V., Peterson, C.D., 2010. Partitioning of sediment on the shelf offshore of the Columbia River littoral cell. Mar. Geol. 273, 11–31.
Vanderburgh, S., Roberts, M.C., Peterson, C.D., Phipps, J.B., Herb, A., 2010. Holocene transgressive and regressive deposits of the Columbia River littoral cell barriers and beach plains. Mar. Geol. 273, 32–43.
Woxell, L.K., 1998. Prehistoric Beach Accretion Rates and Long-Term Response to Sediment Depletion in the Columbia River Littoral Cell. M.S. Thesis, Portland State University, Portland, Oregon (206 p).